UNIVERSITÀ DEGLI STUDI DI BOLOGNA

Facoltà di Ingegneria
Corso di Laurea Magistrale in Ingegneria Meccanica

Dipartimento di Ingegneria Industriale

Tesi di Laurea in Laboratorio di Meccanica dei Tessuti Biologici

The behaviour of osteocyte dendritic processes in bone under cyclic load

Candidato:
Simone Maria Mulargia

Relatore:
prof. Luca Cristofolini

Correlatori:
prof. David Taylor
prof. Giangiacomo Minak
ing. Rita Stagni

Anno accademico 2012-2013

A Martina
A Maria Cristina
A Maria Carlotta

A Model must be wrong, in some respects, else it would be the thing itself.
The trick is to see where it is right.
[H. A. Bent]

Summary

Bone is continually being removed and replaced through the actions of basic multicellular units (BMU). This constant upkeep is necessary to remove microdamage formed naturally due to fatigue and thus maintain the integrity of the bone. The repair process in bone is targeted, meaning that a BMU travels directly to the site of damage and repairs it. It is still unclear how targeted remodelling is stimulated and directed but it is highly likely that osteocytes play a role. A number of theories have been advanced to explain the microcrack osteocyte interaction but no complete mechanism has been demonstrated.

Osteocytes are connected to each other by dendritic processes. The "scissors model" proposed that the rupture of these processes where they cross microcracks signals the degree of damage and the urgency of the necessary repair. In its original form it was proposed that under applied compressive loading, microcrack faces will be pressed together and undergo relative shear movement. If this movement is greater than the width of an osteocyte process, then the process will be cut in a "scissors like" motion, releasing RANKL, a cytokine known to be essential in the formation of osteoclasts from pre-osteoclasts. The main aim of this thesis was to investigate this theoretical model with a specific focus on microscopy and finite element modelling. Previous studies had proved that cyclic stress was necessary for osteocyte process rupture to occur. This was a divergence from the original "scissors model" which had proposed that the cutting of cell material occurred in one single action.

The present thesis is the first study to show fatigue failure in cellular processes spanning naturally occurring cracks and it's the first study to estimate the cyclic strain range and relate it to the number of cycles to failure, for any type of cell.

Rupture due to shear movement was ruled out as microcrack closing never occurred, as a result of plastic deformation of the bone. Fatigue failure was found to occur due to cyclic tensile stress in the locality of the damage. The strain range necessary for osteocyte process rupture was quantified. It was found that the lower the process strain range the greater the number of cycles to cell process failure.

FEM modelling allowed to predict stress in the vicinity of an osteocyte process and to analyse its interaction with the bone surrounding it: simulations revealed evident creep effects in bone during cyclic loading.

This thesis confirms and dismisses aspects of the "scissors model". The observations support the model as a viable mechanism of microcrack detection by the osteocyte network, albeit in a slightly modified form where cyclic loading is necessary and the method of rupture is fatigue failure due to cyclic tensile motion. An in depth study was performed focusing on microscopy analysis of naturally occurring cracks in bone and FEM simulation analysis of an osteocyte process spanning a microcrack in bone under cyclic load.

Table of contents

List of figures

Chapter 1

Introduction

1.1 Bone cells

There are four types of cells in bone tissue: osteoclasts, osteoblasts, osteocytes and bone lining cells (Figure 1.1). Each is essential for the growth and maintenance of bone.

Osteoclasts are giant multinucleated cells derived from the monocyte / macrophage family (Suda et al. 1999). They are responsible for the removal of damaged or diseased bone and are a key player in bone remodelling (Boyle et al. 2003).

Osteoblasts are mononuclear cells and are responsible for initial bone formation as well as later bone remodelling (Ducy et al. 2000). The main function of osteoblasts is to synthesise and secrete type 1 collagen, proteoglycans and glycoproteins necessary for the formation of osteoid, the unmineralized, organic portion of the bone matrix that forms prior to the maturation of bone tissue (Neve et al. 2011). Once osteoblasts have performed their duty and synthesised the new osteoid, 50% - 70% of the osteoblast cell population undergo apoptosis, i.e. programmed cell death, with the remainder differentiating into either bone lining cells or osteocytes (Franz-Odendaal et al. 2006, Lynch et al. 1998).

Bone lining cells are flat, elongated cells believed to be derived from osteoblasts. They cover over 80% of the bone surface. These cells are inactive in terms of remodelling or modelling activities and are directly apposed to the bone surface. They are vital in the maintenance of mineral homeostasis in the bone and function in the exchange of ions between bone fluid and interstitial fluid (Miller and Jee 1987).

Osteocytes are old osteoblasts that occupy the lacunar space and are surrounded by the bone matrix. They possess cytoplasmic dendrites that form a canalicular network for communication between osteocytes and the bone surface. Long time regarded as simply a cell at the end of its lifetime, embedded in a mineral matrix, the osteocyte is now seen as the cell at the center of and the initiator of the bone

remodelling process (Bonewald 2007). It is believed osteocytes sense strain within bone and are stimulated to elicit a suitable response to it.

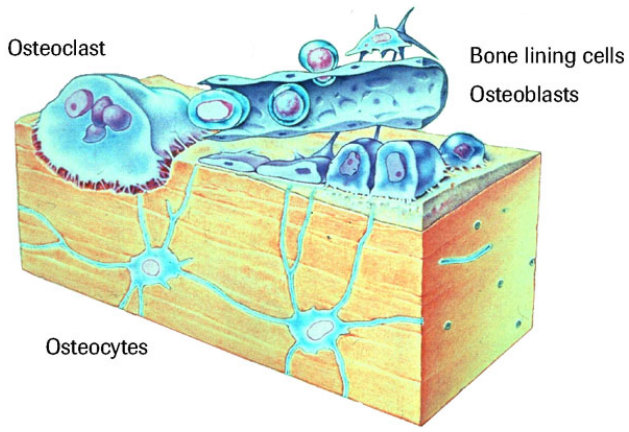

Figure 1.1. This image shows bone cells disposure in the osseous tissue: osteocytes are embedded within the bone matrix, whereas osteoclasts, osteoblasts, and lining cells are present at the bone surface.

1.2 The osteocyte and its properties

Osteocytes constitute the main cellular component of mammalian bones. Osteocytes represent more than 95% of all the bone cells (20,000 to 80,000 cells/mm3 of bone tissue); there are approximately 20-fold more osteocytes than osteoblasts in a bone (Marotti 1996, Franz-Odendall et al. 2006). In human bone, Frost estimated that the mean half life of osteocytes is 25 years (Frost 1966).

The role of osteocytes remained unknown for a long time and was probably underestimated. Over the last 15 years, many publications have aimed to highlight the role of these cells. Osteocytes are distinctive and individual cells that are embedded within the bone matrix, whereas osteoclasts, osteoblasts, and lining cells are present at the bone surface.

1.2.1 Morphology

Osteocytes have a dendritic morphology, i.e. branched projections, while their cell body has fusiform shape in long bones or sometimes rounded in flat bones (Figure 1.2) (Vasta et al. 2008). These cells are localized in osteocytic lacunae, small cavities within the bone matrix, and have been buried in the matrix (Manolagas 2006). They present some cytoplasmic "extensions": the dendrites that extend into channels in the matrix called "the canaliculi". Osteocytes communicate with each other and

with the cells at the surface of the bone tissue via these dendrites (Palumbo 1990). The lacuno-canalicular system which represents only 1% of interstitial fluid volume constitutes a molecular exchange surface area which has been estimated at 400-fold higher than the Havers and Volkmann system and 133-fold higher than the trabecular bone system (1,200 m^2 versus 3 and 9 m^2), respectively for rat male (Bronner 1992).

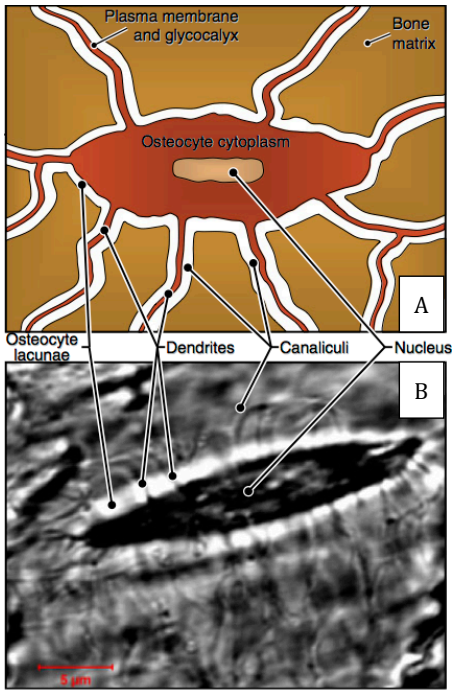

Figure 1.2. This picture shows a schematic representation of an osteocyte (A) and confocal microscopy imaging of an osteocyte from rat tibia (B).

Some studies have shown that according to the type of bone formed and the activity of the osteoblasts involved, the newly formed osteocytes can adopt a variable size and morphology in comparison with older osteocytes already embedded in the matrix (Marotti et al. 1994). Moreover, the morphology of embedded osteocytes is dependent on the bone type. Indeed, osteocytes found in trabecular bone are more rounded than osteocytes from cortical bone (Currey 2003), with the latter adopting an elongated morphology (Currey 2003). In humans, osteocytes measure approximately 10 μm across the short axis and 20 μm along the long axis in long bones (Noble 2008).

The cytoplasmic processes are approximately half the diameter of the canaliculi, with murine canaliculi ranging between 50 and 100 nm in diameter (Zhang et al.

2006). Osteocytes display polarity in terms of the distribution of their cell processes with the majority coming from the cell membrane facing the bone surface (Palumbo et al. 1990).

1.2.2 Attachment of Osteocyte Cell Processes to the Bone Matrix

In order for osteocytes to perceive mechanical information and regulate bone remodelling accordingly they must be anchored to their extracellular matrix (ECM) (McNamara et al. 2009).

To date the nature of this attachment is not completely understood. Osteocytes are embedded in mineralized bone matrix, but maintain a pericellular space (50–80 nm) to facilitate fluid flow and transport of metabolites. This provides a spatial limit for their attachment to bone matrix. Integrins are cell adhesion proteins that may play a role in osteocyte attachment. However, integrin attachments require proximity between the ECM, cell membrane, and cytoskeleton, which conflicts with the osteocytes requirement for a pericellular fluid space.

McNamara *et al.* showed in their studies (McNamara et al. 2009) that the canalicular wall is wave-like with periodic conical protrusions extending into the pericellular space. Cell bodies are immediately surrounded by a layer of pericellular matrix and do not contact the walls of their lacunae directly. In contrast, osteocyte processes contact walls of canaliculi, but only at discrete spots where specialized protrusions ("hillocks") bulge from the mineralized matrix (Figure 1.3). These local connections of the osteocyte process to the surrounding bone matrix are the so called 'focal adhesions'.

1.3 The mechanical properties of cells

The mechanical properties of cells are reported to be regulated by a range of factors including interactions with the extracellular environment and other cells, differentiation status, the onset of pathological states, as well as the intracellular factors, for example, the cytoskeleton (Kelly et al. 2011).

A variety of techniques are available for measuring cellular stiffness, including atomic force microscopy (Sato et al. 2004; Schrot et al. 2005; Costa et al. 2006), micropipette aspiration (Deguchi et al. 2005), optical trapping (Henon et al. 1999), microplate compression (Caille et al. 2002), and magnetic bead twisting/pulling (Wang and Ingber 1995; Laurent et al. 2002; Karcher et al. 2003; Feneberg et al. 2004; Matthews et al. 2004; Overby et al. 2005).

Usually biological materials show viscoelastic behaviour but they may be referred to as elastic if we limit their analysis to a certain level of stress/strain. The Young's

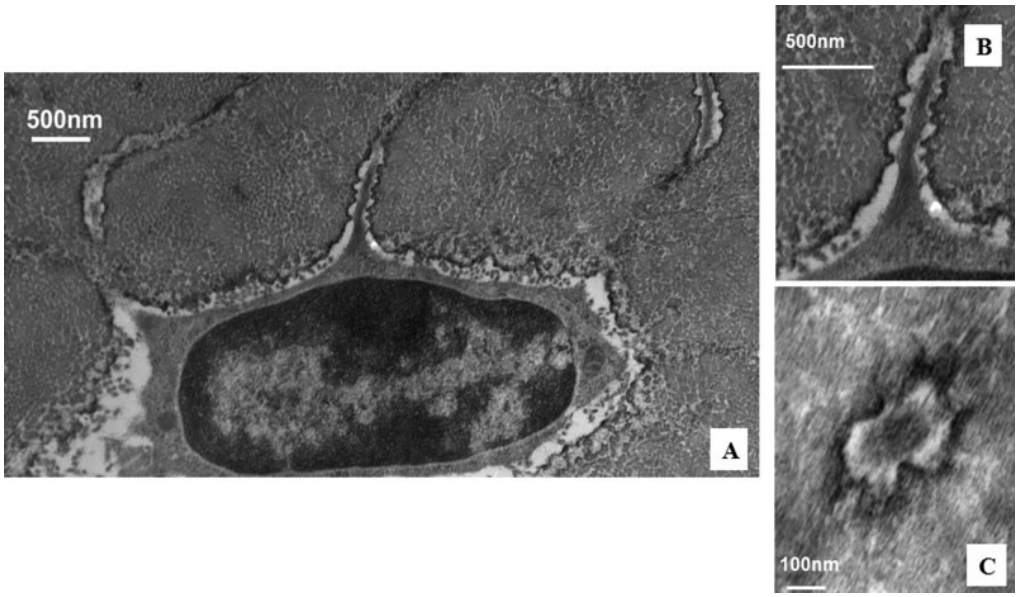

Figure 1.3. TEM photomicrograph of osteoctye (A) shows osteocyte and enlarged longitudinal (B) and cross-sections (C) of cell process showing that the bony wall of the canaliculus has protrusions ('hillocks') projecting from the wall completely across the pericellular space to contact the cell membrane of the osteocyte process.

modulus value for biological material was noted to fall in the range 0-200 kPa, as stated by Radmacher in his studies (Radmacher 1997).

Zeng *et al.* (2009) estimated the effective Young's modulus of elasticity of normal Schlemm's canal (SC) endothelial cells, combining magnetic pulling cytometry of isolated cultured cells with finite element modelling of the mechanical response of the cell to traction forces. Their results showed that the upper bound for the effective Young's modulus of elasticity of the cultured SC cells ranged between 1,007 and 3,053 Pa (Zeng et al. 2009).

Kelly *et al.* (2011) estimated the elastic modulus of MC3T3-E1 osteoblasts: Atomic Force Microscopy (AFM) was employed to investigate the influence of cell cycle phase on mechanical properties of cells. Cells were seeded on sterile glass slides and adhered to them. Then, cells were indented with an AFM tip and elastic modulus values were determined using Hertian analysis.

Cells in the G1 phase had an average elastic modulus of 3.5 ± 0.3 kPa, compared with an average of 5.9 ± 0.5 kPa for cells in the S phase (Kelly et al. 2011).

Cells need to be able to withstand the many stresses and strains that they are exposed to as they travel around and function within the body. Many types of cells are believed to act as mechanosensors, perceiving mechanical forces and converting them into biosignals to stimulate the necessary action (Kim et al. 2009).

There is much knowledge on the elastic and viscoelastic properties of cells and their membranes but we know very little about how the mechanical forces animal cells experience interact with, and possibly damage the cell membrane. This lack of knowledge is due to the difficulty of conducting this type of testing.

One of the few exceptions is mechanical testing by pipette aspiration, a method used in a number of studies of red blood cells and the mechanical forces necessary to cause membrane rupture (Rand and Burton 1964, Rand 1964).

Sheldon *et al.* measured the adhesion of osteoblast-like MC3T3-E1 cells to silicate and borate glasses using colloidal probe microscopy (Sheldon et al. 2011).

In the present study it was assumed that the stress necessary to cause the rupture of cells adhesion to glass in Sheldon *et al.* tests (i.e. 7.96 Pa) is the same as the shear stress necessary to break the focal adhesions between osteocyte processes and bone matrix (as illustrated in section 1.2.2).

1.4 Fatigue failure

Fatigue failure is described as the failure of a material due to cyclic loading. It usually occurs where the loading a material is experiencing is too low to cause instantaneous rupture under monotonic loading but yet is at a certain critical level. At this level, repeated loading and unloading can cause the formation of a microscopic crack at a stress concentrator. For bone this could be a cement line, interlamellar debonding, canaliculi or osteocyte lacunae (Carter and Hayes 1977, Vashishth et al. 1997, Curry 2002). Overtime this crack will propagate until it reaches a critical size and the material suddenly fractures. Generally the higher the stress applied the lower the number of cycles to failure.

1.5 Microcracks in bone

Frost (1960) was the first to identify microcracks in bone. He described small cracks of linear morphology, in the order of 30 – 100 μm in human rib bone (Frost 1960). He hypothesised that these small cracks were formed as a result of fatigue damage caused by cyclic loading *in vivo*. To ensure that what he was seeing was cracks formed *in vivo* and not artefacts due to preparation of the specimens, Frost designed a method, still used today, to identify microcracks and separate them from artefacts. Basic fushin, a stain that binds non specifically to exposed calcium, was applied to a bone sample prior to any preparation. This stain coated the edge of microcracks already present at the point of staining. Microcracks formed later, during preparation, would have no stain and so artefacts could be separated from true *in vivo* microcracks. This method has been validated many times over, by many researchers

(Burr and Stafford 1990, Burr et al. 1997b, Burr and Hooser 1995) and refined using heavy metal staining, applying lead-uranyl acetate in conjunction with backscatter electron detectors in a scanning electron microscope (Figure 1.4) (Schaffler et al. 1994).

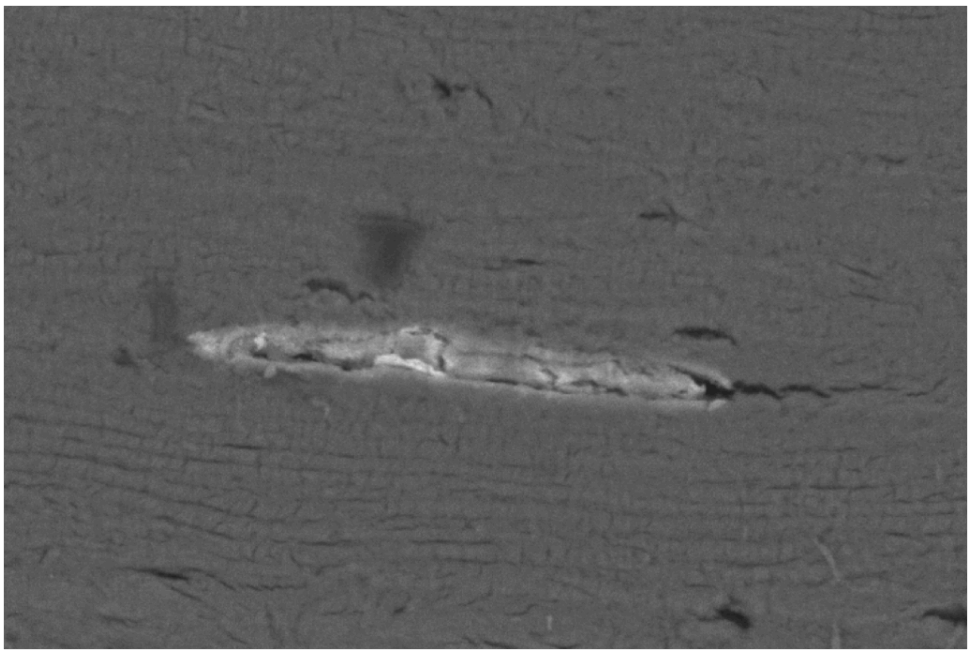

Figure 1.4. Heavy metal bulk staining imaged using a backscatter electron detector: the halo of stain surrounding the crack in bone proves that the crack imaged was formed *in vivo*.

Microdamage is believed to form naturally due to everyday activities such as walking and running. Bone, like any other weight bearing material, will amass fatigue induced damage after cyclic loading. If this damage was allowed to build up, failure of the material would occur within a matter of months (Taylor et al. 2004).

Microcracks are believed to serve two functions in dealing with the load a body experiences. Firstly, it is proposed that interaction between microcracks and bone cells triggers the re-modelling sequence and secondly, the production of microcracks is a method by which bones take the energy they experience with load and disperse it (Schaffler et al. 1994).

A number of experimental studies have linked microdamage to cyclic loading of bone. Forwood removed rat tibia from five groups of animals exposed to different levels of load and an increasing number of cyclic loads and demonstrated that crack

density was dependent on the level of loading the bone was exposed to and that cracks develop *in vivo* due to cyclic loading (Forwood and Parker 1989).

Bone can fail in fatigue in as few as 1000 – 100,000 loading cycles at strain ranges of 5000 – 10,000 microstrain. The average peak physiological strain is generally much lower, typically less than 1500 microstrain in tension and 2500 in compression (Rubin 1984, Schaffler et al. 1989).

Microcracks are elliptical in shape. They have an average longitudinal length of 400 μm and an average length in the transverse direction of 100 μm. The mean aspect ratio of longitudinal to transverse length is 4 : 1 (Lee et al. 2000). This implies that cracks will take advantage of the anisotropic grain of bone material and grow longest in the direction propagation is easiest, longitudinally (Hazenberg et al. 2006a). The average inclination of a microcrack is 70° to the longitudinal axis of the bone (Taylor et al. 2003). Cracks tend to initiate at areas of stress concentrations, where discontinuities are present within the material (Reilly and Currey 1999, Reilly 2000). Burr and Stafford developed criteria to identify microcracks under a light microscope: they should have a sharp border, a halo of stain surrounding the crack, be longer than canaliculi, smaller than vascular canals, be stained through the depth of the section, have well stained edges and less stain in the intervening space (Burr and Stafford 1990).

1.6 Microdamage and bone remodelling

Frost suggested that remodelling could occur to repair damage in bone (Frost 1960).

To prevent possible failure of the bone, microcracks are repaired by the targeted actions of basic multicellular units (BMU). This is an orchestrated group of cells, composed of an osteoclast, which removes damaged bone, and an osteoblast, which lays down new, healthy bone.

Fatigue damage provides a convincing signal as the level of damage will provide a direct measure of the risk of failure (Taylor 1997). Burr conducted an experiment to observe if the frequency of BMU resorption cavities and microcracks in adult dogs, exposed to 3 point bending at 1500 microstrain for 10,000 cycles, was higher than would be expected from random remodelling processes. They found microcracks were associated with resorption spaces six times more often than expected by chance alone (Burr and Martin 1993). To determine if remodelling followed the accumulation of microcracks or whether microcracks formed in areas of pre existing resorption due to increased stresses in the area a second experiment was conducted. Three point bending load was applied to left forelimbs of dog models. Eight days later the right forelimb was exposed to the same forces and the dog was immediately sacrificed. The results showed equal numbers of microcracks in each limb radius but significantly more resorption spaces and more resorption spaces associated with cracks in the

left limb (Mori and Burr 1993). This was as expected if damage is targeted and supported a cause and effect association between damage and repair.

1.7 Osteocytes as mechanosensory cells

It is poorly understood how bones detect the presence of a microcrack initially, but due to their position and quantity within the bone osteocytes have been proposed as major players in this process (Cowin et al. 1991, Lanyon 1993). Frost referred to the proposed osteocyte response to mechanical stimuli as a mechanosensory mechanism (Frost 1987). Their number, location and ability to communicate with each other along with studies that demonstrate that an increase in damage accumulation is associated with areas of low osteocyte numbers (Mori et al. 1997), makes them a highly likely candidate.

Some experimental evidence has been produced to support this hypothesis. Fatigue failure has been shown to take place when osteocytes are not present as with radiation induced osteocyte death (Melanotte and Follis 1961) and avascular necrosis (Kenzora et al. 1978). Dunston produced evidence that loss of osteocyte number was associated with hip fractures (Dunstan et al. 1993) and Qiu produced results which showed that microcrack accumulation is related to areas of osteocyte reduction in aging human bone (Qiu et al. 1997).

You *et al.* concluded that mechanically stimulated osteocytes release RANKL, a cytokine which has been shown to bind to RANK on the surface of osteoclast precursors and has the potential to stimulate osteoclastogenesis (You et al. 2008, Boyle et al. 2003). Microdamage would be expected to directly injure osteocytes, disrupt their attachment to the bone matrix, interrupt their communication network of processes and canaliculi and alter their metabolic exchange (Burr et al. 1985, Schaffler 2003).

There have been a number of hypotheses put forward as to how osteocytes and microcracks interact in order to stimulate the formation of a BMU and initiate the targeted remodelling process. These include apoptosis (Verborgt et al. 2000, Noble and Reeve 2000, Noble et al. 1997, Kurata et al. 2007, Seeman 2006), fluid flow (Nicolella et al. 2006, You et al. 2008), the primary cilum (Anderson et al. 2008, Malone et al. 2007, Temiyasathit and Jacobs 2010) and rupture of cell process by shearing motion (Taylor et al. 2003, Hazenberg et al. 2006).

The main aim of this thesis was to investigate on the hypothesis that the rupture of cell processes by shearing motion leads to the initation of the targeted bone remodelling process, as suggested by Taylor *et al.* (Taylor et al. 2003) in the 'scissors model' theory presented in the next section.

1.8 "The scissors model": rupture of osteocyte cellular processes

Osteocyte process rupture has been shown to be associated with microcrack formation. After fatigue tests on living bone, osteocyte cells and their dendritic processes were disrupted, suggesting that they may experience failure in the vicinity of matrix damage (Colopy et al. 2004, Frost 1960). Taylor et al. (2003) proposed a cellular transducer in damage stimulated bone remodelling whereby osteocyte processes could be cut by a shearing motion between crack faces. Under applied compressive loading microcrack faces will be pressed together and will undergo relative shear motion. If this motion was > 0.2 μm, or the width of a process, then the cell process would rupture (Figure 1.5). This hypothesis was put forward based on a theoretical model developed using analytical and numerical methods. It was suggested that once the osteocyte processes were ruptured they could secrete passive and active cellular material into the extra cellular matrix which could diffuse through the matrix and be detected elsewhere, possibly leading to BMU formation and bone repair (Taylor et al. 2003).

The theoretical model was first described by Taylor et al. using fracture mechanics (Taylor et al. 2003). It was developed to predict the relative movement of crack faces and from this to predict if it was possible for osteocyte processes to be ruptured due to crack face displacement. The equation was derived from an equation for a 2D crack as no equation was available for a 3D crack (Ewald and Wanhill 1989).

$$\delta T = \frac{2\sigma}{E}(1-\nu^2)\sqrt{a^2-x^2} \tag{1.1}$$

Here δT is the tensile opening (i.e. the separation of the crack faces), σ is the applied tensile stress, E is the osteocyte Young's modulus, ν is Poisson's ratio, a is the half-length of the crack and x is the distance along the crack, measured from the crack centre. Maximum displacement occurs in the middle of the crack therefore $x = 0$.

The equation evolved to take into account the two crack dimensions for an elliptical crack, i.e. the minor and major axes, a and b, as well as the two major types of load a crack could be influenced by compression and tension (Taylor et al. 2003).

$$\delta T(z) = \left(f\left(\frac{b}{a}\right)^{0.1} \left(\frac{a}{b}\right) \frac{\sigma}{E}(1-\nu^2)\sqrt{a^2-x^2} \right) * cos(\beta)cos(\beta) \tag{1.2a}$$

$$\delta s(z) = \left(f\left(\frac{b}{a}\right)^{0.1} \left(\frac{a}{b}\right) \frac{\sigma}{E}(1-\nu^2)\sqrt{b^2-z^2} \right) * sin(\beta)cos(\beta) \tag{1.2b}$$

$$\delta T(x) = \left(f\left(\frac{b}{a}\right)^{0.1} \frac{\sigma}{E}(1-\nu^2)\sqrt{a^2-x^2} \right) * cos(\beta)cos(\beta) \tag{1.2c}$$

$$\delta s(x) = \left(f\left(\frac{b}{a}\right)^{0.1} \frac{\sigma}{E}(1-\nu^2)\sqrt{a^2-x^2} \right) * sin(\beta)cos(\beta) \tag{1.2d}$$

Here δT(x) is the tensile displacement of the crack faces along the x axis and δT(z) is the tensile displacement along the z axis (which will be zero in compressive loading): δS is the corresponding shear displacement. β describes the angle of the crack to the long axis of the bone, which is also the axis of applied tensile or compressive stress.

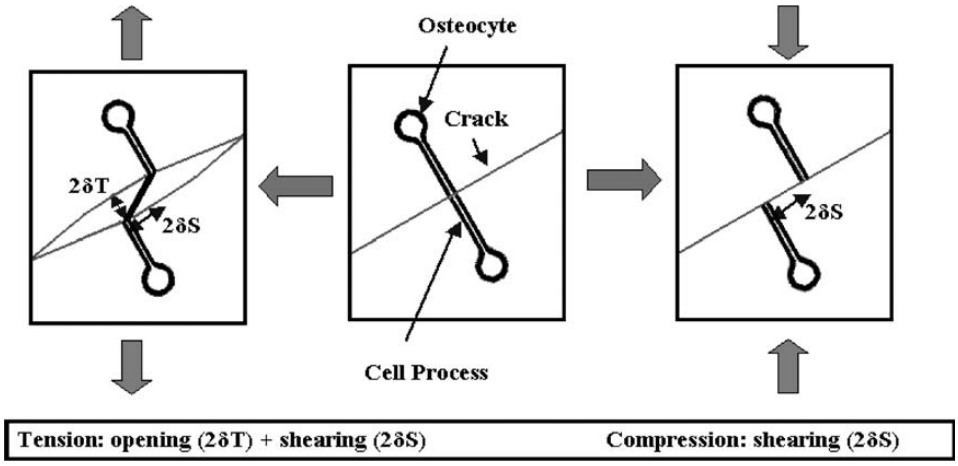

Figure 1.5. Cell processes spanning a crack can be stretched and cut by tensile or compressive loading, due to relative displacements of the crack faces. (Taylor et al. 2003).

The work went on to predict the failure of osteocyte processes across cracks in both tension and compression. The simplest case (and the one thought to be most common in practice) was compression, in which case failure was assumed to occur if the crack face shear displacement was $2\delta S > 0.2$ μm i.e. the typical diameter of an osteocyte process. If crack face displacement is greater than the width of an osteocyte process then the process would rupture. This equation was used to predict at what crack size osteocyte processes would begin to rupture. At a crack length of

30 μm no cellular processes failed, even at loading above that normally experienced *in vivo*. A 100 μm crack would begin to see failure at 28 MPa and a crack of 300 μm would produce cell process failure at 10 MPa. It was concluded that as crack length and applied stress increased so too did cell rupture. A normal crack exposed to high loading and a large crack exposed to normal loading would result in cell process rupture (Taylor et al. 2003). This work was purely theoretical with no experimental proof. To confirm the findings experimental testing was required.

These predictions fitted very well with experimental data generated on repair stimulation for cracks of different sizes. Experimental work was conducted to investigate whether microcracks could rupture osteocyte cellular processes. Cellular material was observed crossing the crack face and the rupture of this cellular material was also visualised using phalloidin (a stain specific to F actin) a fluorescent antibody stain and confocal microscopy (Hazenberg et al. 2006a). These studies confirmed that local damage of processes, in isolation from other proposed stimuli such as cyclic strain and fluid flow, could stimulate a remodelling response.

The findings on microdamage are in agreement with the work of Taylor *et al.* (2003) and suggest that the number of broken cellular processes may be a viable mechanism by which bone is able to estimate cracks size and elicit a suitable and targeted response.

Dooley (2013) tested this model and its predictions, supporting the "scissors model" as a viable mechanism of microcrack detection by the osteocyte network (Dooley 2013). Her study represents the first time osteocyte fatigue failure has been quantified. The main aim and achievements of her studies were as follows:

- The first aim was to identify material spanning a microcrack and conclude that it was osteocyte cellular material and not collagen fibres: Phalloidin staining of f-actin confirmed that the fibres identified as osteocyte cell processes were as believed and not collagen fibres (Dooley 2013).

- The theoretical model suggested that the degree of osteocyte processes rupture would depend on microcrack size: smaller microcracks would experience very little rupture while large microcracks would experience huge amounts of cell damage. This prediction was tested and Dooley's analysis demonstrated that as crack size increased so too did the number of ruptured processes. This was in accordance with the hypothesis: the bigger the crack the more urgent the need for repair and the more broken processes the more biochemicals that would be released into the bone matrix, therefore the bigger the stimulation for repair.

- The mathematical equations generated to predict the number of broken processes for cracks of varying lengths were tested. Experimental data on the number of intact processes per millimetre of crack length were plotted against

theoretical curves based on the model. Dooley did this for a number of animal types so that certain parameters in the model would need to be changed. The experimental data and the theoretical curves, for the three species of animal studied (i.e. bovine, murine, ovine), fit well. There was a degree of scatter in the data but most could be explained if it is assumed that intact cellular processes along a microcrack are in a Poisson distribution (Dooley 2013). The analysis demonstrated that the general trend of the collected results can be predicted using fracture mechanics theory based on "scissors model".

- The theoretical scissors model advanced that cell processes spanning microcracks of varying sizes would be more likely to break if they were exposed to increased cyclic compressive stresses. Results from Dooley's thesis proved that cyclic loading is the main mode of rupture and stated that the number of ruptured osteocyte cellular processes is a function of crack length, applied stress and number of cycles. The longer the microcrack and the greater the applied stress the fewer osteocyte processes that remain intact.

- The scissors model suggested shear stress as the method by which cell processes ruptured. It was believed that under compressive loading the microcrack faces would be pushed together and the crack would close. With continued compression the microcracks would slip and undergo shear movement cutting the cells as a scissors would. Dooley's studies showed that complete microcrack closing did not take place as previously believed: processes ruptured because of stress and strain resulting from cyclic compressive loading, not because of microcrack complete closure.

- After supporting the "scissors model" as a viable mechanism of microcrack detection by the osteocyte network, Dooley wanted to ensure the appropriate cellular response for targeted modeling was activated by cell process rupture. This testing was performed in vitro using an osteocyte type cell line (MLO-Y4) and the application of a planar defect. Apoptosis of cells and RANKL production was stimulated by cutting of MLO- Y4 cell process as the "scissors model" predicts. These are the essential criteria for initiation of bone remodelling, suggesting that the "scissors model" is a viable means of stimulating targeted remodelling.

1.9 Aims of this study

The main aim of this project was to investigate on the "scissors model" as proposed by Taylor *et al.* (2003). The model suggested that it is possible to cut osteocyte cellular processes, where they pass across microcracks, by shear movement generated

by cyclic compressive strains. It is believed that the rupture of osteocyte cellular processes in the vicinity of a microcrack may be a way by which the presence of the microcrack is identified, the severity of it is signalled and if necessary the formation of a BMU to target the damage for repair is prompted.

Dooley showed evidence that process rupture takes place in cyclic compressive loading and calculated the displacement range for tested processes, suggesting that as the displacement of the area surrounding an osteocyte process increases the number of cycles to osteocyte process failure decreases (Dooley 2013).

I wished to test the "scissors model" and its predictions. In particular the aim of my project was to use both microscopic and finite element modelling (FEM) techniques to test various aspects of the model and add results to Dooley's research. The aims were as follows:

- I wanted to investigate microcracks formed *in vivo* and test bone samples under loading comparable to *in vivo* stress, in contrast with Dooley's research, which focused on cracks formed by notching samples. Microcracks in bone are usually oriented longitudinally and I applied load in this direction, while Dooley applied compressive load perpendicularly to cracks.

- I wanted to test bone samples that had not been frozen, to compare with Dooley's samples, which had always been frozen before testing.

- I wanted to measure the displacement of the area of *in vivo* cracks surrounding an osteocyte process under cyclic compressive loading. I wanted to investigate on its effect on process failure, following the same analysis procedure as Dooley in her work.

- I wanted to create a FEM model of an osteocyte process spanning a microcrack in bone, in order to get reliable results on process strain and predict crack displacement.

- I wanted to convert all crack displacement values (both from the present study and from Dooley's research) into process strain values, for better fatigue failure analysis and quantification.

Chapter 2

Materials and Methods

2.1 Bovine Bone

Bovine tibia bone was obtained from animals that were skeletally mature and free from bone disease. The bones had been subjected to only free range normal *in vivo* loadings. The bone was kindly supplied by Kepac Abbattoir (Clone, Co. Meath, Ireland). All specimens were stored at 4°C prior to preparation.

2.2 Specimen preparation

The epiphysis and metaphysis of the bone were removed using a hand saw. Then, the specimens were cut transversely to the long axis of the bone, into sections of approx 4 - 5 cm (Figure 2.1). This allowed the specimens to be clamped for cutting with a diamond saw (Struers, Minitron).

Next specimens of bone needed to be prepared for *in situ* straining. The bone was cut into sections 20 mm x 5 mm x 1 mm from the longitudinal axis of the bone (Figure 2.2). 30 specimens were obtained out of one bovine bone tibia.

The specimen thickness of 1 mm worked best for longitudinally notched specimens, thicker sections made it difficult to control crack growth (Hazenberg et al. 2006a). Figure 2.3 indicates loading direction in relation to the bone axis.

Once cut each specimen was assigned a specimen number and exact measurements were taken from each edge of the specimen using a vernier calipers. The data was compiled on an excel spread sheet. The surfaces of the specimens were manually ground flat using silicon carbide paper (400 and 1200 grade).

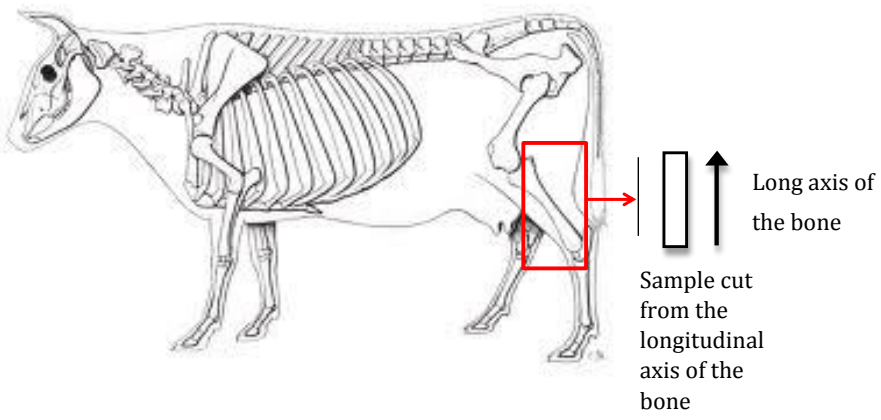

Figure 2.1. Diagram indicating the tibia of a bovine skeleton and showing the orientation of the specimens cut for in situ strain testing.

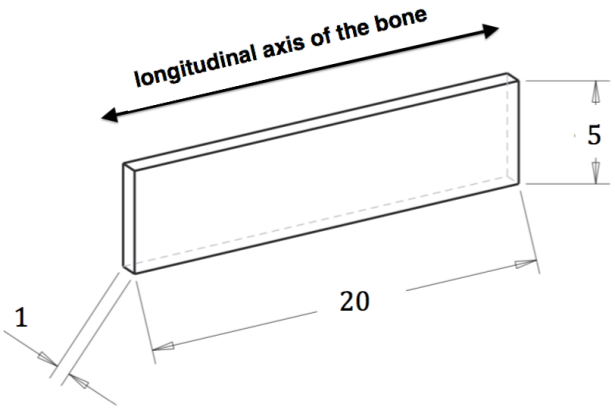

Figure 2.2. Diagram showing specimen orientation.

2.3 Heavy Metal Staining of Bone specimens

It is possible for artefact microcracks to form when a bone is being prepared for analysis, for example due to shrinkage during drying. These microcracks are indistinguishable from *in vivo* microcracks but may not behave like them as the artefact microcracks (formed during preparation of the specimen) would have had no exposure to *in vivo* cyclic loading.

To identify *in vivo* formed microcracks heavy metal bulk staining was performed. This staining was performed en bloc prior to subsequent processing. As a result only microcracks present before the following treatments would be stained. When the specimens were viewed using a backscatter detector in a SEM *in vivo* microcracks could

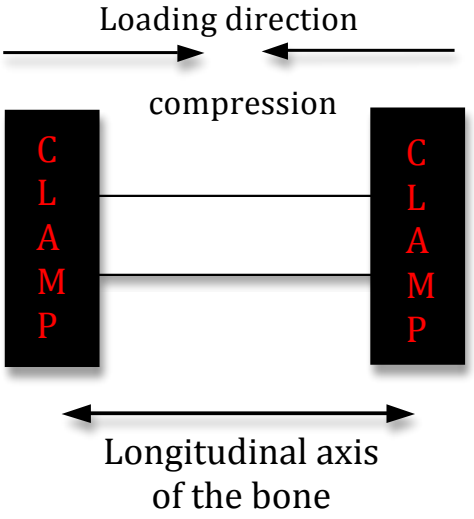

Figure 2.3. Diagram showing the orientation of the bone specimen in the *in situ* loading stage.

be differentiated from artefacts due to a halo of heavy metal staining surrounding them (Figure 2.4).

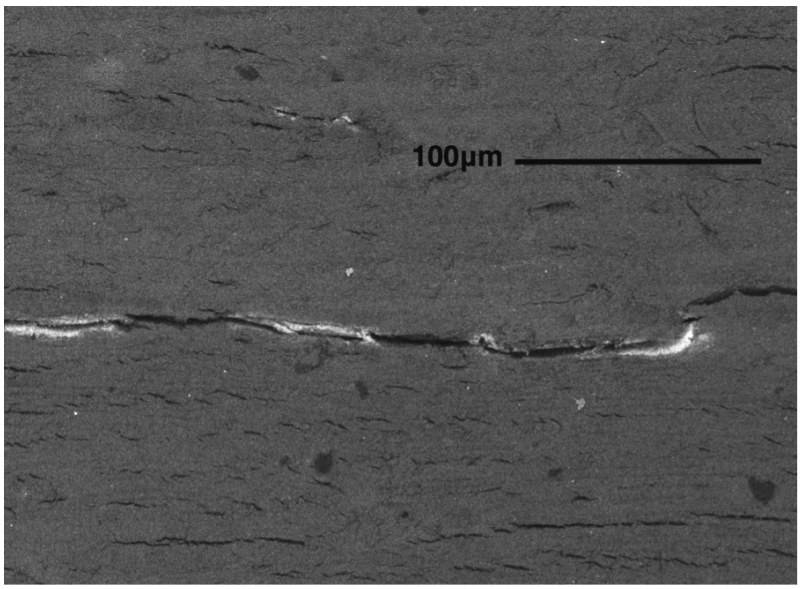

Figure 2.4. SEM image using a backscatter electron detector showing a halo of heavy metal stain surrounding a microcrack. This indicates the microcrack did not form as a result of specimen processing. A number of unstained microcracks can be seen around the haloed microcrack.

This staining process was performed as follows. The specimens were placed in a solution of 70% acetone containing a lead – uranyl acetate complex (20% lead acetate in 70% acetone and 8% uranyl acetate in 70% acetone) (all Sigma Aldrich. Airton Road, Tallaght, Dublin 24) and left for 8 days at room temperature. The solution was gentle shaken daily to prevent sediment settling. The sections were rinsed in 70% acetone and placed into a solution of 1% ammonium sulphide in 70% acetone for 7 days in order to form lead and uranyl sulphide precipitates. The solution was refreshed after three days. The specimens were rehydrated with distilled water for 48 hours (As per method by (Schaffler et al. 1994)).

2.4 Preparation for SEM Analysis

In order to preserve biological specimens from decay, they were fixed in 4% paraformaldehyde for 24 hours at 4 °C. The paraformaldehyde was prepared as follows; 100ml of PBS (Sigma Aldrich. Airton Road, Tallaght, Dublin 24) was poured into a measuring cylinder and 4 g of paraformaldehyde (Sigma Aldrich. Airton Road, Tallaght, Dublin 24) was added in a fume hood. The solution was placed on a hotplate with a magnetic stirrer and the solution was heated gradually. When the solution changed from cloudy to clear it was ready. It was allowed to cool and stored at 4°C. After fixation the specimens were washed three times in PBS to remove all traces of the fixative.

For SEM, a specimen is normally required to be completely dry, since the specimen chamber is at high vacuum. In order to obtain completely dried specimens, they were then alcohol dehydrated in a series as follows; 10% for 10 mins, 30% for 10 mins, 50% for 10 mins, 70% for 10 mins, 90% for 10mins, 100% for 15 mins x 2. Next the specimens were critical point dried (CPD) (Quorum E3000 CPD). The specimens were remeasured once dry to ensure there were no drastic changes in size due to the drying process. No significant differences were found.

2.5 *In situ* straining of bone specimens and SEM Imaging

The whole procedure follows the same steps previously validated by Dooley in her thesis (Dooley 2013).

The Deben in situ stage is a straining stage capable of working within the high vacuum chamber of a SEM. It has a maximum loading ability of 200 N and can be used for either tensile or compression testing. The specimens were mounted in the in situ stage (Figure 2.5) and clamped on either side, with the longitudinal axis parallel to the direction of the applying load.

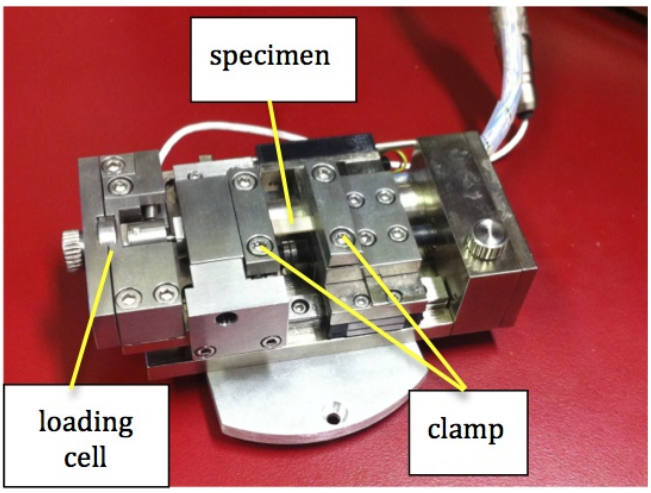

Figure 2.5. The Deben in situ straining stage with specimen mounted in it.

The stage, with the specimen in place, was then loaded into the SEM chamber.

The specimens were imaged in a Tescan MIRA XMU VPFESEM using a backscatter electron detector at an electron voltage of 20 KV. For each specimen stained microcracks were identified and imaged. The microcracks imaged were selected randomly from those formed away from the outer and inner edges of the specimen.

Once a microcrack was identified as an *in vivo* damage the detector was swapped to a secondary electron detector and the electron voltage was dropped to 5 KV. The change of detector allowed for a better resolution to be obtained. This was sometimes necessary to separate individual osteocyte processes. The *in vivo* cracks detected were imaged at low magnification prior to any cyclic strain being applied; these images incorporated the entire length of the microcrack. Higher magnification images were taken of all intact osteocyte processes spanning the microcracks face and the location of each process was recorded to allow observation of this area after cyclic strain was applied to the specimen.

Crack length and crack opening were measured using ImageJ (freeware available online for download). The numbers of intact cell processes spanning the microcrack face were counted manually using the high magnification sequential images.

Cyclic compression was applied at a maximum of 180 N and a minimum of 1 N, generating stress of a maximum of 36 MPa and a minimum of 0.2 MPa, up to the point of process rupture or 100 cycles if the process did not break. At the maximum and minimum load of each cycle the osteocyte process and its surrounding area was imaged, up to the time where the process ruptured (Figure 2.6).

Crack length, number of intact cellular processes and crack opening local to the process of interest were measured using these images. All data was automatically

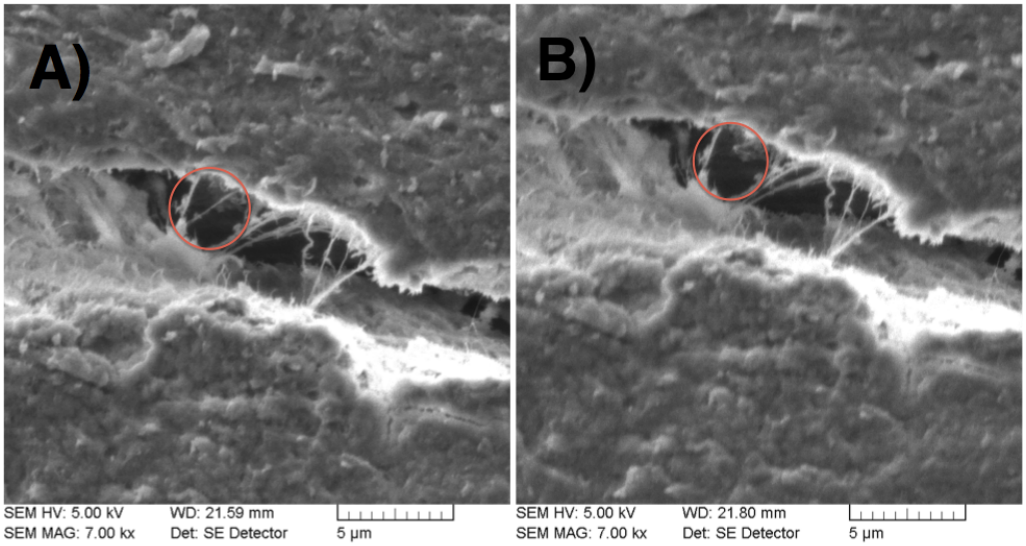

Figure 2.6. SEM images showing the effect compressive loading has on osteocyte processes spanning a microcrack. (A) Prior to any loading – intact processes are present. (B) After one loading cycle – the highlighted process has ruptured, while the other processes remain intact.

transferred to a Deben computer programme linked to the stage. This effectively allowed fatigue testing of osteocyte processes spanning a microcrack.

The displacement range of the microcrack opening was calculated for each osteocyte process observed, up to the point of rupture. To calculate the displacement range the average crack opening at the maximum loading of 180 N and the average crack opening at the minimum loading of 1 N were found. The average minimum was subtracted from the average maximum, giving the difference in the average maximum and the average minimum (Figure 2.7), giving the average displacement range for the area surrounding the osteocyte process. The cycles to failure was not the number of externally applied cycles but was the number of cycles experienced locally by the osteocyte process. The average displacement range of crack edges was then plotted against the number of local cycles to failure.

2.6 FEM Model

A FEM model of an individual osteocyte process spanning a microcrack in bone was realized using the software Ansys Workbench v.14 (Figure 2.8), with the aim of predicting strain in the process and crack opening displacement under cyclic load in accordance with experimental values from Dooley's thesis. The main purpose was to model average conditions of work for an osteocyte after the propagation of a

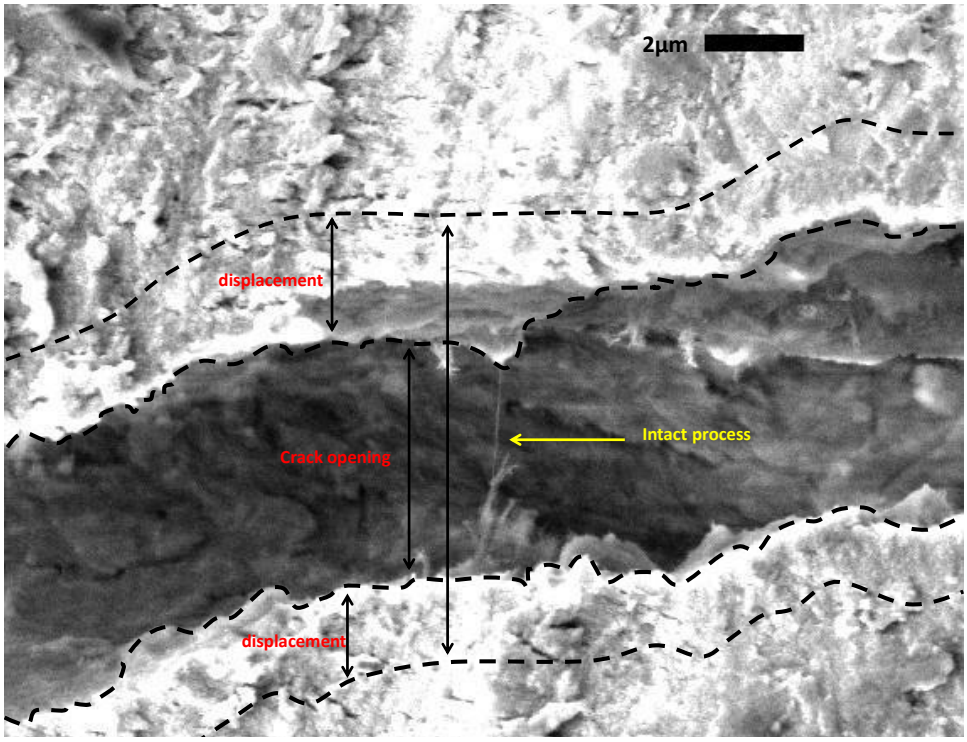

Figure 2.7. SEM image of part of a microcrack, showing an intact process, indicating the crack opening displacement under compressive loading and (schematically) how this changed when the loading was removed.

microcrack in its vicinity. The osteocyte process was modelled as a cylinder of 0.2 μm diameter (in accordance with Taylor et al. 2003), connecting two spheres of 5 μm radius (the two osteocytes), which are distant 37 μm. So, the actual length of the process was 37 μm minus twice the cell radius, i.e. 27 μm. Taking advantage of symmetrical properties, only half of it was modelled, considering the whole osteocyte process being divided into two symmetrical parts by a plane perpendicular to the crack surface. The whole process was stuck into two plates 160 mm x 500 mm x 20 mm from the longitudinal axis of the bone. Both of them were bonded to a larger plate 340 mm x 1000 mm x 20 mm from the longitudinal axis of the bone. The area of contact between the two small plates had no constraints. In this way, the three plates modelled a crack in the bone matrix, whose actual length was 320 μm (twice the 160 μm dimension of the small plates, considering symmetry). The other dimensions of the plates were calculated considering the crack density in the bone matrix being 1 crack/mm^2 (Taylor et al. 2003).

Two different materials were created with the software in order to have different mechanical properties for the osteocyte process and the three plates modelling

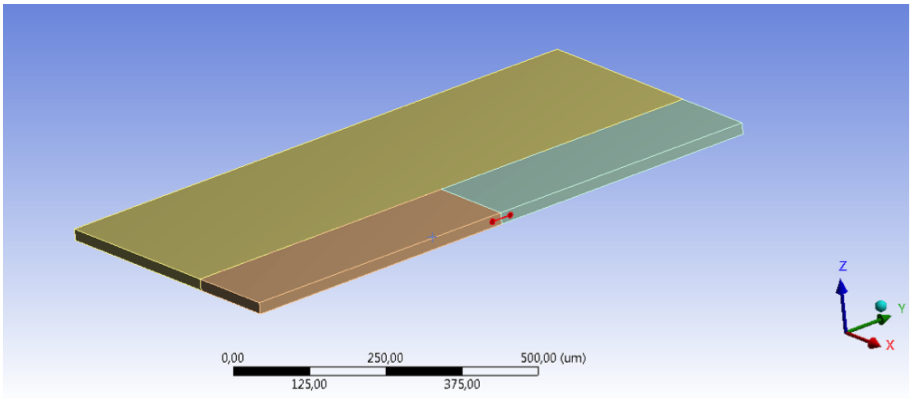

Figure 2.8. ANSYS image of the model showing the two small plates connected to a large plate to model a microcrack in bone, with the osteocyte in red stuck into them.

the surrounding bone matrix. Bone properties were taken from previous publications (Reilly and Burstein 1975, Rimnac et al. 1993), as well as osteocyte material strength properties (Ker et al. 2000, Taylor et al. 2003). Bone modelled as a plastic material, while the osteocyte as an elastic linear material. All the mechanical properties applied to the two different materials are grouped in Figure 2.9.

After creating the geometry, loads and constraints were applied to it. Frictionless supports were applied to the model in order to allow displacement only in one direction, parallel to the main axis of the osteocyte process. Loads were modelled as a pressure on the two opposite surfaces of the bone matrix, both on the larger plate and the smaller plates, as in Figure 2.10, in order to simulate a tensile/compression stress applied to the crack.

2.7 FEM Model Validation

In order to validate the FEM model a comparison with results obtained with formula taken from the literature was made. At first, focus was put on the stress concentration factor in the area surrounding the crack tip. Considering a small edge crack of length a in an infinite plate the stress intensity factor is calculated by the Equation 2.1 (Tada et al. 1985), being K the stress intensity factor and $\sigma$the tensile stress applied to the plate.

$$K = 1.12\sigma\sqrt{\pi a} \tag{2.1}$$

Considering the area close to the crack tip and focusing on a plane passing exactly in the middle of the crack, the stress distribution (assuming the material

Properties of Outline Row 3: Bone

	A	B	C
1	Property	Value	Unit
2	Orthotropic Elasticity		
3	Young's Modulus X direction	22000	MPa
4	Young's Modulus Y direction	15000	MPa
5	Young's Modulus Z direction	12000	MPa
6	Poisson's Ratio XY	0,3	
7	Poisson's Ratio YZ	0,11	
8	Poisson's Ratio XZ	0,21	
9	Shear Modulus XY	5300	MPa
10	Shear Modulus YZ	6300	MPa
11	Shear Modulus XZ	7000	MPa
12	Bilinear Isotropic Hardening		
13	Yield Strength	40	MPa
14	Tangent Modulus	356	MPa
15	Norton		
16	Reference Units (Length, Time, Temperature, Force)	um, s, K, uN	
17	Creep Constant 1	9,56E-17	
18	Creep Constant 2	5,2	
19	Creep Constant 3	0	
20	Tensile Yield Strength	40	MPa
21	Compressive Yield Strength	40	MPa
22	Tensile Ultimate Strength	53	MPa
23	Compressive Ultimate Strength	53	MPa

Properties of Outline Row 4: Osteocyte

	A	B	C
1	Property	Value	Unit
2	Isotropic Elasticity		
3	Derive from	Young's Mo...	
4	Young's Modulus	5900	Pa
5	Poisson's Ratio	0,39	
6	Bulk Modulus	8939,4	Pa
7	Shear Modulus	2122,3	Pa

Figure 2.9. ANSYS screenshot of the mechanical properties for the two different materials of the model: bone tissue and osteocyte.

completely elastic) is described by the Equation 2.2 (Tada et al. 1985), where the stress σ_x depends on the distance r from the crack tip.

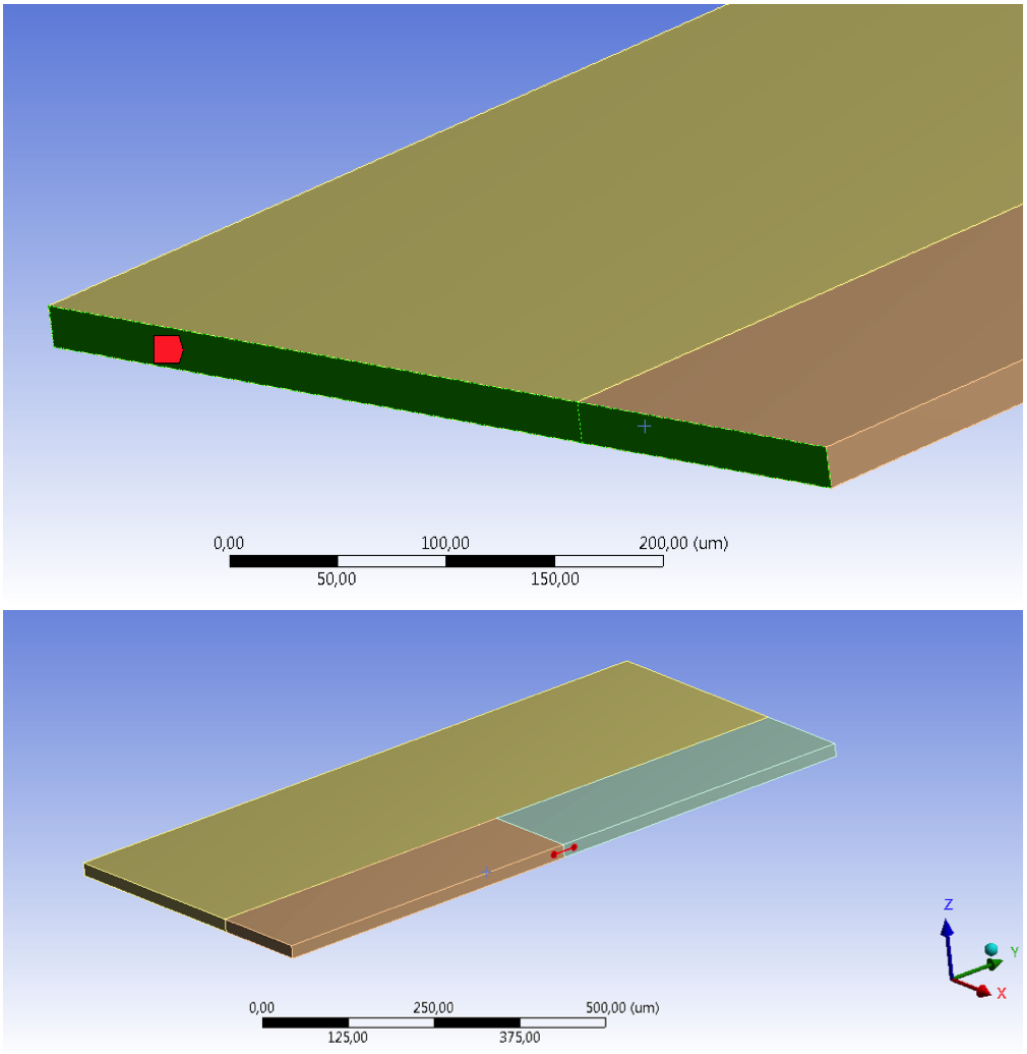

Figure 2.10. Ansys images showing load applied to the model to simulate tensile or compressive loading on a microcrack in bone.

$$\sigma_x = \frac{K}{\sqrt{2\pi r}} \tag{2.2}$$

According to Equation 2.2 the stress value σ_x goes to infinity when the distance from the crack tip r goes to 0 (so at the crack tip), even if in the reality some plasticity reactions occur to limit that value.

To validate the FEM geometry, the model was considered as working in a completely elastic field: all the values related to plasticity were omitted from the material properties, in order to compare the results with theoretical predictions for elastic materials. Focusing on points close to the crack tip, FEM stress values were compared

with theoretical results.

Secondly, focus was put on the crack opening displacement (COD). Equation 2.3 (Janssen et al. 2004) predicts the opening of a crack, showing its dependence on the distance from the crack tip, where E is the Young modulus of the material and ν the Poisson's ratio (considering the material operating in a completely elastic field).

$$\delta(x) = 2u_y(x) = \frac{(1+\nu)(3-4\nu+1)}{E}\sigma\sqrt{2a(a-x)} \tag{2.3}$$

The opening of the crack in the middle of its length was calculated using Equation 2.3 and the result was compared with the crack displacement from the FEM model.

2.8 FEM Simulation

At the first stage, a tensile stress was applied to the model in order to make the crack open and the process increase its length (Figure 2.11). In particular, a series of simulations was run, one for each process on which data had previously been collected during the SEM analysis, in order to make the crack displacement measured in the model match the initial crack opening calculated from SEM images. At the end of each simulation it was possible to collect data and images on stress and strain in the process and in the area surrounding the crack tip, as well as to measure the crack opening. An important analysis was done on images referring to stress values in the process. In particular, the length of the section (free length FL) where stress value was higher than the limit shear value for osteocyte process adhesion to the bone (as described in section 1.3) was measured for each process and plotted in a graph against crack displacement.

At the second stage, cyclic compressive load was applied to the model. The crack in the model this time had an initial opening set to 1.5 μm, in accordance with the average crack *in vivo* opening values obtained from SEM imaging. Cyclic compressive load was simulated making the pressure applied on the two surfaces of the model moving from a maximum value of 18 MPa to a minimum value of 0.1 MPa (in accordance with values applied during in situ loading). 4 cycles of loading were applied to the model. At the end of the simulation it was possible to collect data and images on stress and strain in the osteocyte process and in the area surrounding the crack tip at each step of the cyclic loading, as well as to measure the crack opening. A graph showing crack displacement from the model over the number of cycles of loading applied was plotted and compared to the graph obtained from SEM analysis in Dooley's studies.

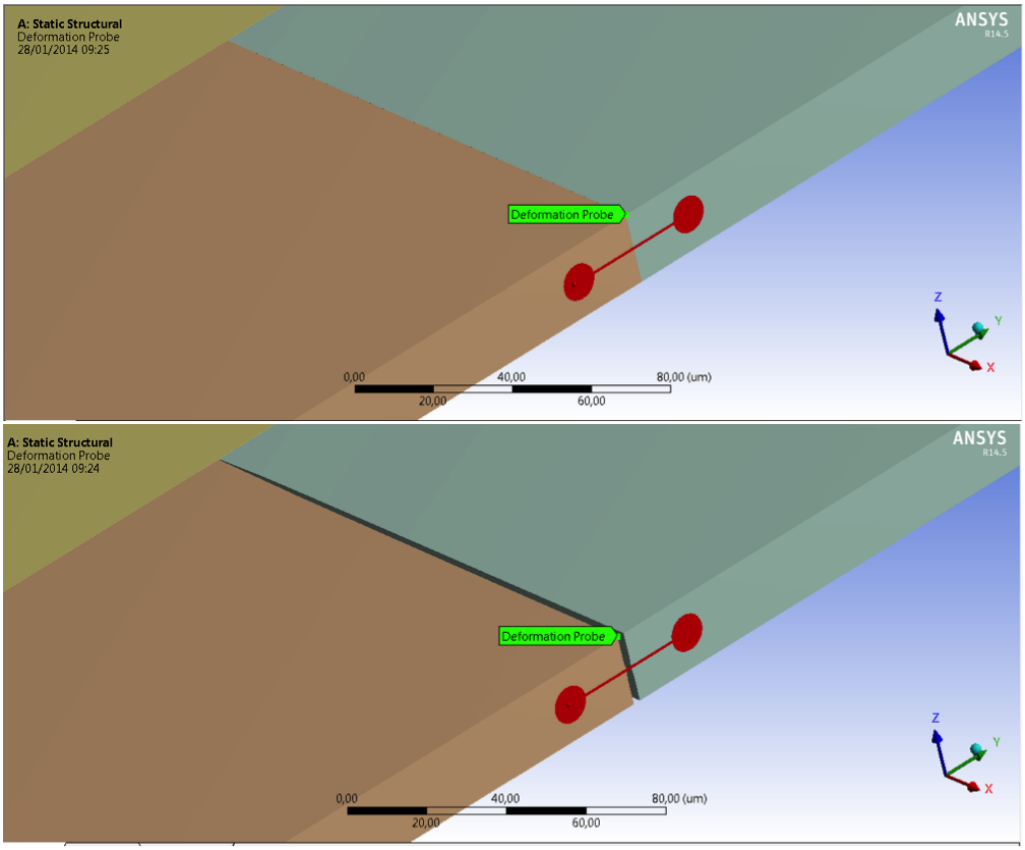

Figure 2.11. Crack opening simulation in the Ansys model: after applying pressure to the unloaded geometry, a gap between the two small plates appear, reproducing the effect of a microcrack in bone opening under tensile load.

2.9 Strain in osteocyte process

Strain for each process was calculated dividing the crack displacement by the free length value obtained in section 2.8, as in Equation 2.4, being ε the longitudinal strain in the process, Δd the crack local opening and FL the free length of the process.

$$\varepsilon = \frac{\Delta d}{FL} \tag{2.4}$$

In this way all crack displacement data could be associated to a precise value of strain in the osteocyte process and all the crack-opening against cycles-of-loading graphs could be converted in strain-in-process against cycles-to-failure graphs.

Chapter 3

Results

3.1 Crack opening over 100 cycles of cyclic compressive loading

According to the "scissors model" under compressive loading the microcrack face should close and undergo shear motion, resulting in the cutting of osteocyte processes spanning the crack face (Hazenberg et al. 2006a). Microcrack opening was observed at one point, randomly chosen, along the microcrack. Observations were made prior to any compressive loading, after one compressive loading cycle and after 100 compressive loading cycles: Figure 3.1 reports results for 10 processes that did not break.

The microcrack opening changed from one cycle to the next and did not appear to follow any type of pattern. In some cases, such as cracks 10 and 2 there was an increase in microcrack opening from *in vivo* loading to 1 cycle. In others, there was a decrease in crack opening. From 1 cycle to 100 cycles the pattern changed again with some samples opening further and others remaining the same. It appeared that opening was not uniform across the length of a crack and that the variations were due to structures in the locality of the microcrack imaged and analysed. In some cases it appeared that compression crushed bridges spanning the microcrack allowing the crack to close further and in other cases the crushing of a bridge allowed the crack to open further as it was no longer tethered to anything.

It was clear from these results that osteocyte cell process rupture did not take place as described in the "scissors model": face closing did not occur in any crack, even after 100 cycles of loading.

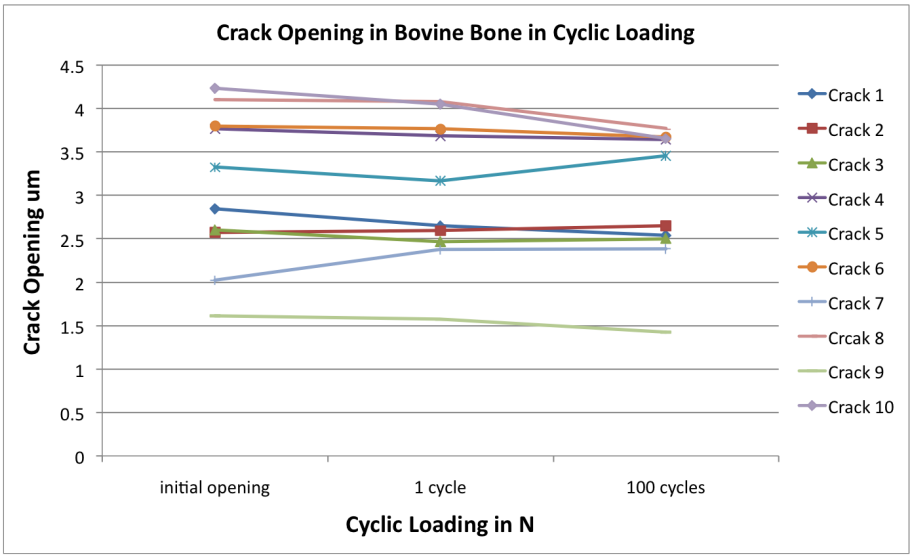

Figure 3.1. This graph indicates the size of crack opening at one point along the microcrack. Measurements were taken prior to any compressive loading, after one cycle of loading and after 100 cycles of compressive loading.

3.2 Individual osteocyte process rupture and microcrack displacement in the locality

Data from SEM images were used to determine how the maximum and minimum compressive stress of each cycle affected the area immediately surrounding an intact process. The main aim was to monitor what changes occurred in microcrack displacement immediately prior to the process rupturing and at what cycle the process ruptured.

Figure 3.2 shows the variation in crack opening displacement cycle-by-cycle in the vicinity of each osteocyte process, up to the point that the process ruptured. The osteocyte processes that failed under cyclic loading ruptured very early into the loading sequence. Most of them anyway survived intact after 100 externally applied loading cycles. In particular, 10 processes out of 35 broke, while 25 out of 35 did not experience any failure after 100 cycles. Figure 3.3 shows the variation in crack opening displacement cycle-by-cycle in the vicinity of 5 osteocyte processes that did not break during tests, showing results for cycles 1 to 3 and 97 to 100.

Considering the 10 processes that broke, the maximum number of externally applied cycles before rupture was 5 cycles, that corresponded to 3 local cycles experienced by the process. Compressive loading generally tended to close the cracks, but not completely. In some cases (processes 1 and 4 in Fig. 3.2) crack local opening increased under compressive loading: in this case the shear component of the stress

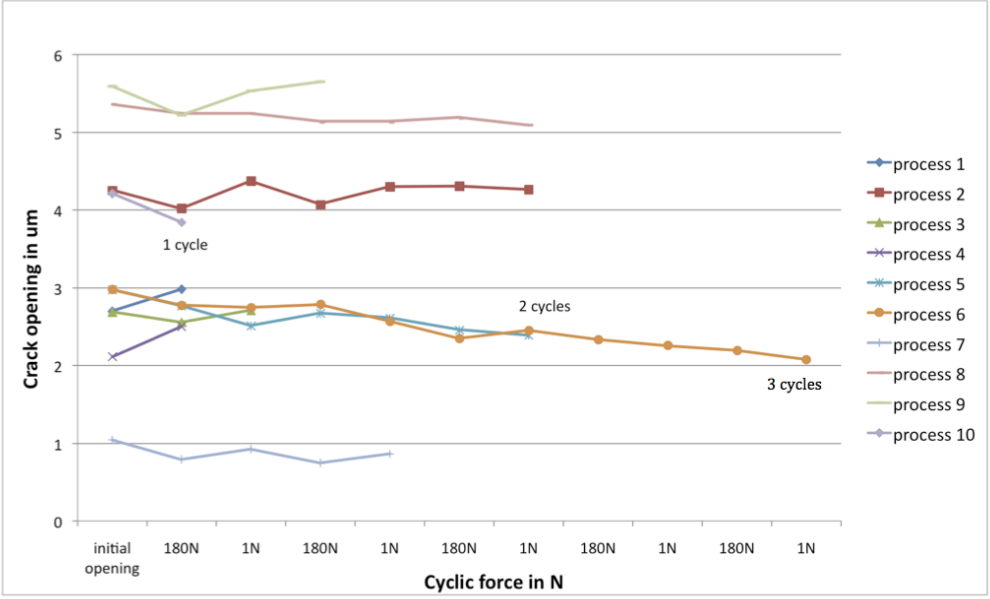

Figure 3.2. This graph shows the crack opening displacement at the maximum (180 N) and minimum (1 N) loading of each cycle, up to the point that the process ruptured.

applied had a relevant role in determining crack displacement.

Over time the average opening tended to decrease but the cyclic displacement range (i.e. the difference between the maximum and minimum in successive cycles) remained approximately constant (Figure 3.4 shows an example). The opening variation is above the limit of the experimental error, i.e. 2% of the measured values.

It appeared that osteocyte processes spanning the areas where the average displacement was greatest ruptured earliest (processes 1, 4 and 10 in Figure 3.2 and Figure 3.5 and those with the smallest variations in crack opening and closing survived intact for longest (processes 2, 6 and 7 in Figure 3.2 and Figure 3.5).

Monotonic rupture on the first cycle occurred three times, at a displacement range between 2 and about 4 μm; reducing the displacement produced failure after increasing numbers of cycles. Failure occurred even at displacement range of about one tenth of that measured for monotonic rupture (process 7 broke after 3 local cycles of loading with a displacement range of 0.342 μm).

These results were generated using samples that, due to necessary SEM imaging, had to be dried. Drying biological material can have an effect on the properties of the material. In order to decide if the processing changed the cellular material to such a degree that it was no longer representative of *in vivo* behaviour, the average displacement of a microcrack, under cyclic compressive loading, for a fully hydrated

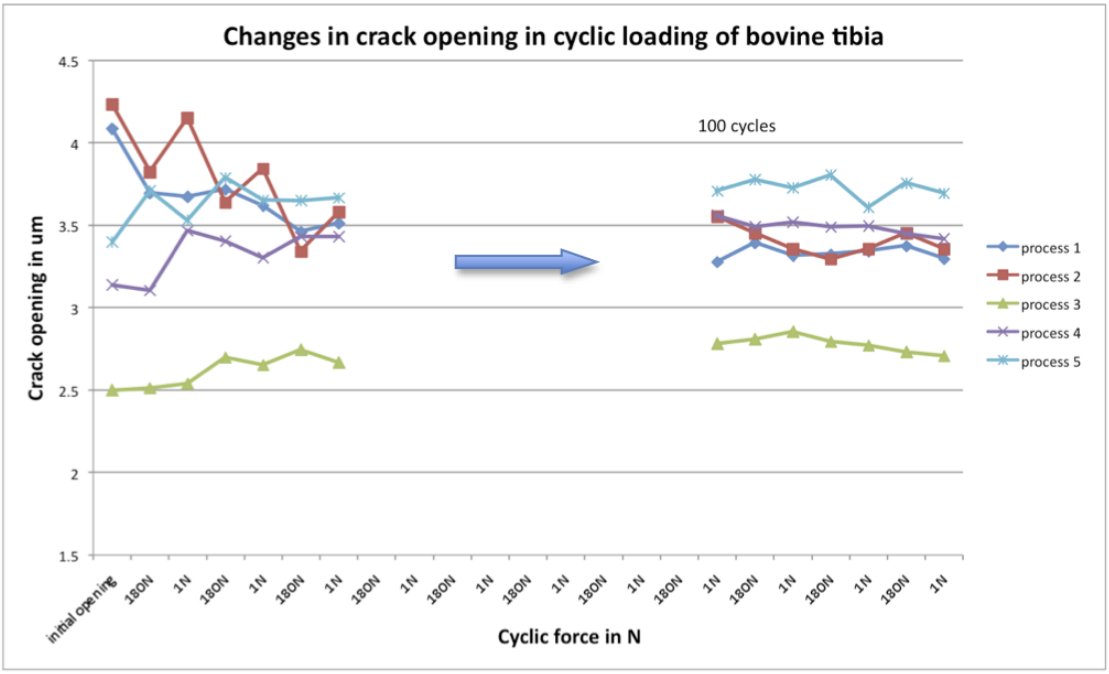

Figure 3.3. This graph shows the crack opening displacement at the maximum (180 N) and minimum (1 N) loading of each cycle for 5 processes that did not break during tests (results are reported for cycles 1 to 3 and 97 to 100).

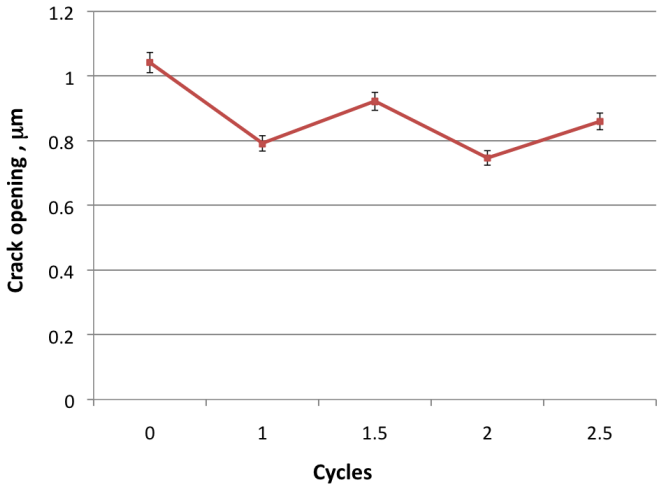

Figure 3.4. An example of results from *in situ* cyclic loading, showing the variation of crack opening displacement cycle-by-cycle in the vicinity of an osteocyte process which ruptured after four cycles. This data refers to process number 7. For each measurement the respective experimental error is represented in black.

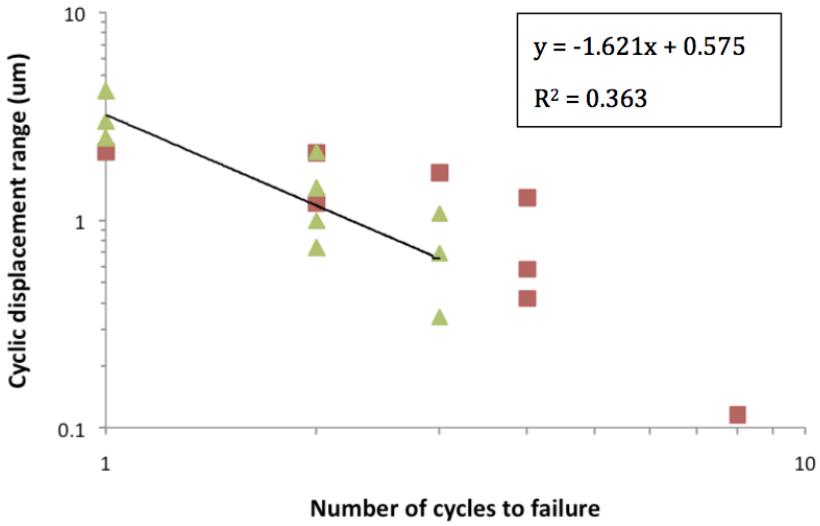

Figure 3.5. This graph shows the cyclic displacement range in the vicinity of each process, calculated as the difference in the average maximum and the average minimum for each process. This is plotted against the number of cycles to failure. Results obtained from Dooley's thesis are included in this graph (red squares).

sample, was estimated by Taylor et al. for 100 cycles for both wet and dry samples, and for 1 cycle for the dry samples, using equations from the previously described theoretical model (Section 1.9), using data generated as part of Dooley's thesis (Dooley 2013, Chapter 3 – Fig. 3.5).

Figure 3.6 shows these results along with the results from the *in situ* testing of individual processes, including the displacement range values for the 10 processes that ruptured during tests and the 5 processes that remained intact after 100 cycles, which had been previously analyzed in Figure 3.6 considering crack opening in their vicinity.

3.3 FEM model validation results

In order to validate the FEM model described in section 2.7 a comparison with results obtained with formula from theoretical calculations was made.

Considering points in the area surrounding the crack tip, FEM stress values resulted to be coherent with theoretical values obtained with Formula 2.1. For example, the theoretical stress value calculated with the Formula 2.1 for a point placed at a distance $r = 10$ μm from the tip (total half crack length, $a = 160\mu$m) was σ= 107.96

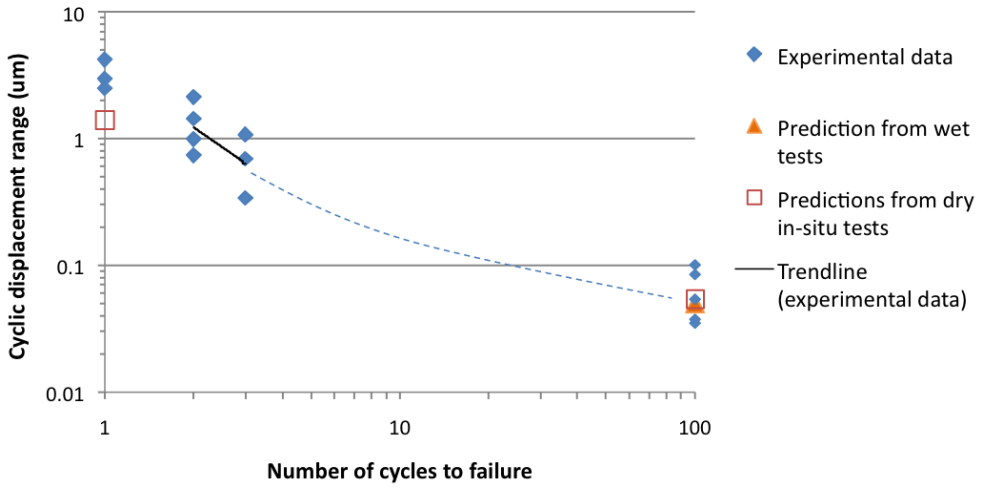

Figure 3.6. Results from the *in situ* fatigue tests on individual osteocyte processes, showing the number of cycles to failure as a function of cyclic displacement range, plotted against the number of cycles to failure. Also included are three estimated results obtained by analysis of the 1 cycle and 100 cycle data set for dry and wet samples (Dooley 2013).

MPa. From the ANSYS model a value of σ= 106.55 MPa was obtained at the same distance from the crack tip.

The opening of the crack in the middle of its length was then calculated using Equation 2.3 and the result was found to be coherent with the crack displacement from the FEM model. Considering $x = a = 160\mu$m, in order to calculate the opening of the crack in the middle of its length, $E = 20$ GPa, ν= 0.39, the following result was obtained from Equation 2.3: $\delta(a) = 0.769\ \mu$m. The crack opening in the same point measured from the ANSYS model with same material elastic properties was $\delta(a) = 0.767\ \mu$m.

After proving both stress and crack displacement values from the FEM model were in accordance with theoretical predictions within the limitation of elastic behaviour of materials, it was assumed that the same model with plasticity properties added to bone material could accurately describe the behaviour of bone tissue under compressive load.

This assumption is important for the analysis of creep effect on crack opening displacement under compressive loading shown in section 3.6.

3.4 Free Length in individual osteocyte process

It was assumed that the adhesion limit shear value between the process surface and the bone surrounding it before they separate under applied load was 7.96 Pa, in accordance with the hypothesis made in section 1.3. A second assumption was that the rupture of the adhesive connection happens during the initial opening of the crack and no further rupture occurs during the *in situ* cyclic loading. As the crack opening range during the loading tests was definitely smaller than the opening cracks experienced *in vivo*, stress values experienced from the osteocyte process during tests could not be higher than *in vivo* stress and so no further connections between the process and the bone could break.

Being the Free Length (FL) for an individual osteocyte process the length of the section where the adhesion to the bone ruptured, simulations run with the FEM model allowed to make estimates of the Free Length values in relation with the crack local *in vivo* opening. Figure 3.7 shows that the Free Length of an individual osteocyte process increases as the crack *in vivo* opening increases, with linear proportionality.

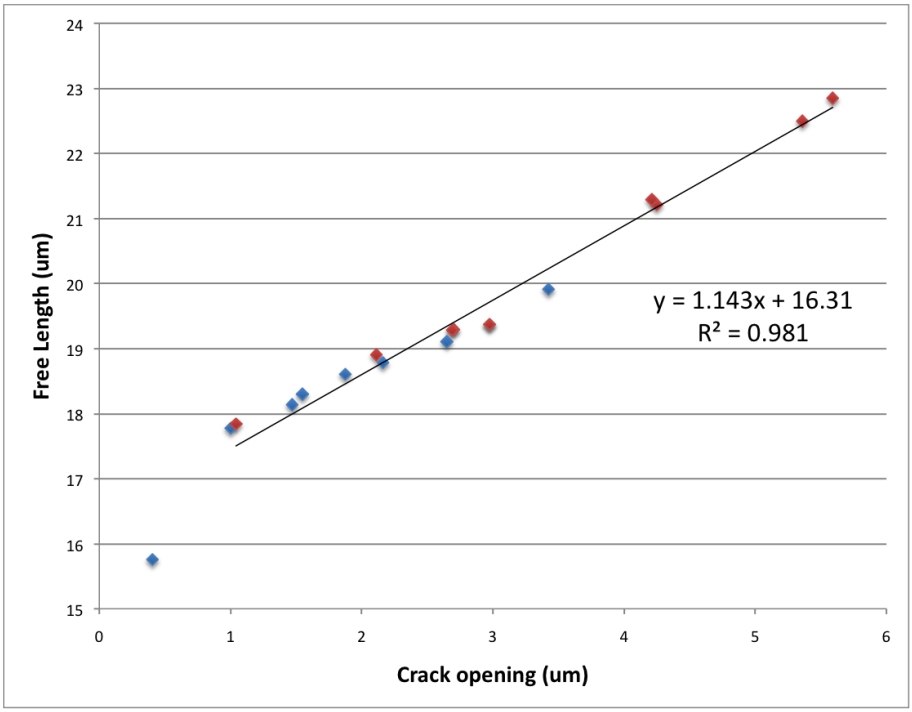

Figure 3.7. Results from the FEM analysis of stress in an individual osteocyte process under tensile load, showing the Free Length of each process as a function of the crack displacement, plotted against the respective crack *in vivo* opening. Values calculated from Dooley's tests are included in the graph (blue points).

3.5 Strain in individual osteocyte process

After obtaining the Free Length values for each tested process, strain in individual osteocyte process during cyclic compressive loading was calculated using Equation 2.4.

Figure 3.8 shows the variation in process strain cycle-by-cycle, up to the point that the process ruptured: it was obtained from Figure 3.2 changing crack displacement values with process strain values.

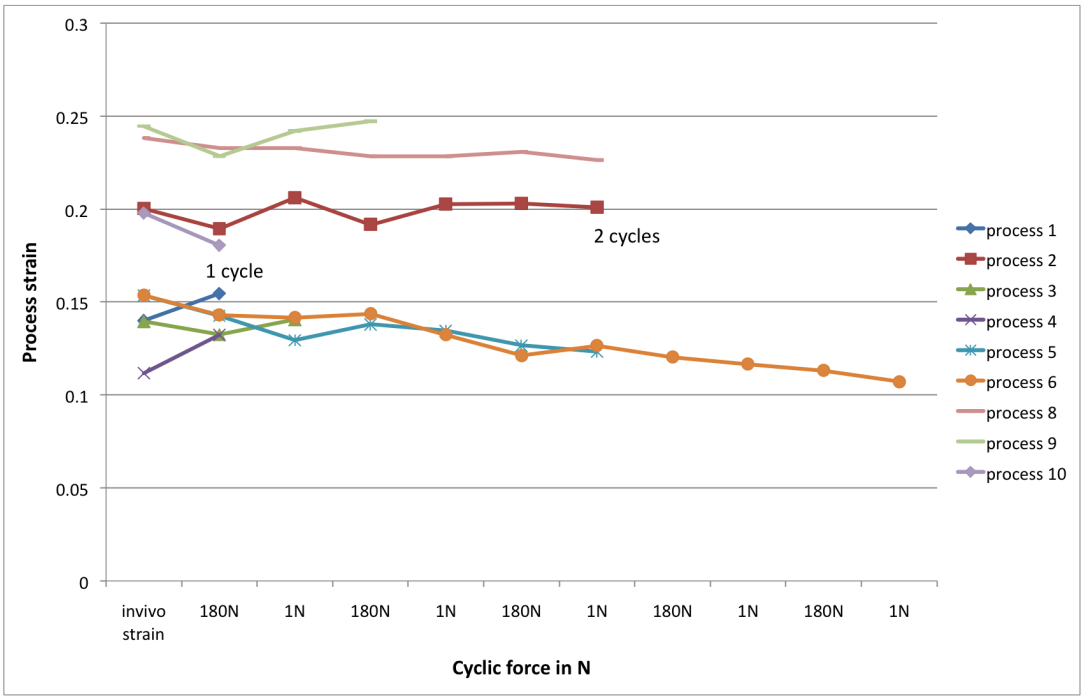

Figure 3.8. This graph shows the strain in osteocyte process at the maximum (180 N) and minimum (1 N) loading of each cycle, up to the point that the process ruptured.

Osteocyte processes spanning the areas where the average displacement was greatest experienced the highest cyclic strain range and ruptured earliest (processes 1, 4 and 10 in Figure 3.8) while for those with the smallest variations in crack local opening and closing, the lowest cyclic range of strain made they survive intact for longest (processes 2, 6 and 7 in Figure 3.8).

Strain values obtained where compared with strain values calculated from Dooley's results. Processes tested in this study experienced levels of strain between a minimum of 0.02 and a maximum of 0.19 (Figure 3.9) while processes tested by Dooley experienced strain levels in a range 0.12 - 0.007. Even if strain levels had

different ranges, both analysis showed the decreasing of the number of cycles to failure with the increasing of cyclic strain range experienced by osteocyte process.

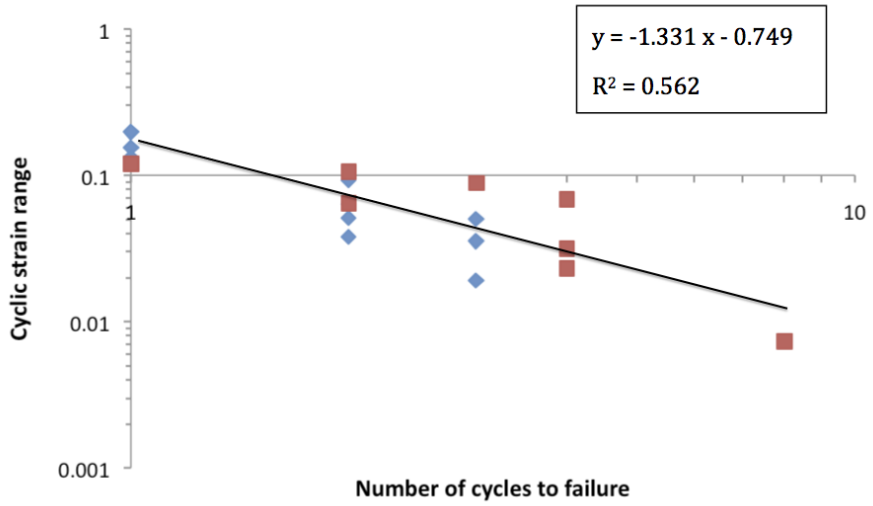

Figure 3.9. This graph shows the cyclic strain range in each process, calculated as the difference in the average maximum and the average minimum for each sample. This is plotted against the number of cycles to failure. Results obtained from Dooley's thesis are included in this graph (red squares).

3.6 Crack opening over cyclic compressive load

As reported in section 3.2, and highlighted in Dooley's analysis too, the average opening of a crack under cyclic compressive load tended to decrease over time but the cyclic displacement range (i.e. the difference between the maximum and minimum in successive cycles) remained approximately constant. The FEM model was used to investigate on this behaviour. It was demonstrated that creep is responsible of this behaviour of cracks in bone under cyclic loading.

In materials science, creep is the tendency of a solid material to move slowly or deform permanently under the influence of mechanical stresses. It can occur as a result of long-term exposure to high levels of stress that are still below the yield strength of the material.

The FEM model showed what happen if only plastic characteristics are considered in modelling the bone tissue: the average opening of a crack tends to remain constant over time (Figure 3.10). In the first cycle of loading plasticity effect occurred in the area surrounding the crack tip, where stress exceeded the yield limit. This made the crack not to come back to its original position once the load was

reduced to 1 N, because some permanent deformation was given to the material. Once the material had rearranged its structure in the area surrounding the crack tip due to plasticity properties, the cyclic application of new 180 N loads did not deform the material permanently any more: then deformation was completely elastic and reversible and the average opening of a crack remained constant over time, in contrast with the behaviour revealed by experimental measurements.

Once the creep effect, as evaluated in bone by Rimnac (Rimnac et al. 1993), was included in the material properties, the FEM model showed the behaviour highlighted by experimental analysis for *in vivo* cracks: the average opening of the crack under cyclic compressive load tended to decrease over time and the cyclic displacement range remained approximately constant, about 0.84 μm in this case (Figure 3.11).

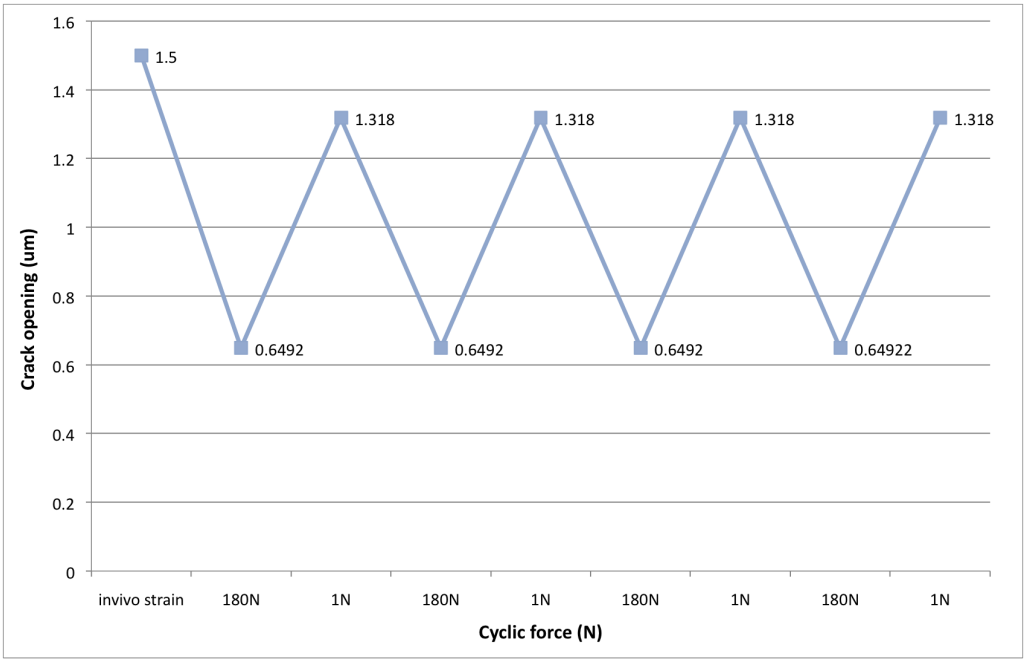

Figure 3.10. This graph shows the crack opening in the FEM model at the maximum (180 N) and minimum (1 N) loading of each cycle. Considering no creep effect in the model makes the maximum and minimum values after the first cycle be constant over time.

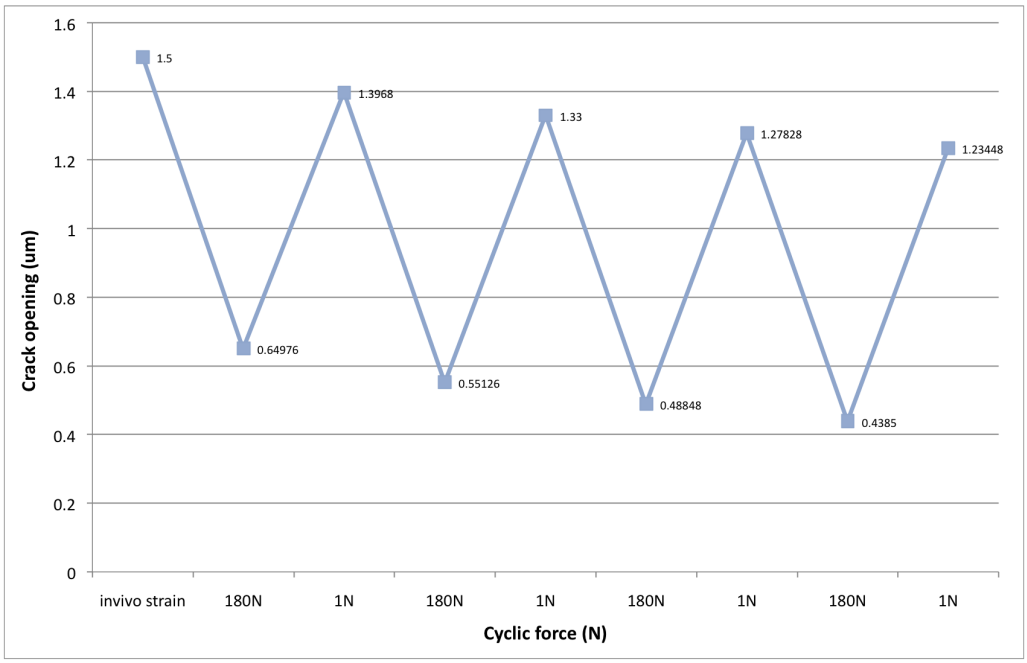

Figure 3.11. This graph shows the crack opening in the FEM model at the maximum (180 N) and minimum (1 N) loading of each cycle. Considering creep effect in the model makes the maximum and minimum values decrease over time maintaining the cyclic displacement range approximately constant.

Chapter 4

Discussion

4.1 Discussion

Microcracks in bone form naturally due to everyday motions associated with movement (Frost 1960). Repair is performed by targeted remodelling, a crucial activity if the integrity of bone is to be maintained (Bentolila *et al.* 1998, Mori and Burr 1993). If these cracks were not repaired the bone would weaken and fail within a matter of months (Taylor *et al.* 2004). The aim of the present work was to add more results to the analysis started by Dooley in her thesis and to create a FEM model as a useful instrument to predict crack displacement and the level of strain in an osteocyte process spanning a microcrack in bone.

Dooley's thesis (Dooley 2013) focused on the rupture of osteocyte processes where they cross the microcrack face and supported the "scissors model" as a viable mechanism of microcrack detection by the osteocyte network. (Taylor 1997).

The "scissors model" was originally proposed as a theoretical model based on mathematical equations. The equations were used to quantify the cell process rupture based on crack size and applied stress, with the results showing that the greater the crack length the greater the number of ruptured processes. Increasing the applied stress would lead to smaller cracks incurring cell damage. It was suggested that under applied compressive loading microcrack faces would be pushed together, leading to a closing of the crack.

The *in situ* straining stage testing allowed more detailed analysis of what changes took place in a microcrack from the initial *in vivo* crack opening displacement, up to 100 cycles of compressive loading. Microcracks analysed had formed *in vivo* and had therefore already been exposed to cyclic compression. This is a reasonable explanation for the high number of processes (25 out of 35) that did not break after 100 cycles of compressive loading: we can suppose that a process that has already experienced cyclic compressive loading *in vivo* and did not break after that, has high

probability to remain intact after the *in situ* loading, considering a stress comparable to *in vivo* conditions (36 MPa, i.e. the stress experienced by bovine tibiae during a run) is applied during the test. The presence of some processes breaking after *in situ* loading shows cellular material can fail due to mechanical fatigue.

These results, together with Dooley results from her thesis (Dooley 2013), are currently the only data showing mechanical fatigue in cellular material. Along with the data showing osteocyte process breaking fatigue failure has been quantified. In particular, this is the first ever study to show fatigue failure in cellular processes spanning naturally occurring cracks.

Microcrack opening analysis results were in accordance with Dooley data from tests . In the present studies samples had not been frozen, while samples from Dooley's tests had been frozen, so the similarity of the two sets of results suggests that freezing did not affect the cell processes. The original proposal for the "scissors model" suggested that once exposed to compressive loading the microcrack faces would be pushed together, resulting in the closing of the crack. Further compression would cause the crack faces to slide against one another causing shear motion. If the shear motion was greater than 0.2 μm, or the width of a cell process, then the cell process would be cut in a scissor like fashion (Hazenberg *et al.* 2006a). This was not found to be the case, with no microcrack closing completely over the course of the 100 cycles (Fig. 3.1).

Crack opening displacement showed the same behaviour Dooley already noticed in her thesis: over time the average crack opening in the vicinity of a process tended to decrease but the cyclic displacement range (i.e. the difference between the maximum and minimum in successive cycles) remained approximately constant (Fig. 3.2).

The *in situ* straining stage study allowed confirmation that osteocyte processes can rupture when exposed to compressive cyclic loading. It showed that a small number of osteocyte processes can break after a single load application.

It was clear that fatigue was the most common method of rupture but rupture at one cycle also took place. As cyclic microcrack opening was suggested to be a cause of fatigue, a very large crack displacement was believed to cause enough disruption to a process to cause a monotonic rupture.

Looking at data collected, a correlation was found between the displacement in an area local to an intact cell process and the number of cycles to failure. The results signify that as displacement of the area surrounding the osteocyte process increased the number of cycles to osteocyte process failure decreased, as noticed by Dooley.

The processes that failed after *in situ* testing appeared to have higher maximum strains and lower strain amplitudes compared to Dooley's results.

In fatigue testing cyclic load is normally described by a constant-amplitude cycle such as a sine wave. Being ε_{max} and ε_{min} the maximum and minimum strains in a cycle, the following three terms can be defined for each cycle of loading:

- Strain range $\Delta\varepsilon = \varepsilon_{max}$-$\varepsilon_{min}$
- Strain amplitude $\varepsilon_a = (\varepsilon_{max}$-$\varepsilon_{min})/2$
- Mean strain $\varepsilon_m = (\varepsilon_{max} + \varepsilon_{min})/2$

The number of cycles to failure is affected both by the strain range and the mean strain. Unfortunately there is no simple way to combine these two as their connection varies depending on the type of material and other factors.

A way to do it for low cycle fatigue is to use the Smith Watson Topper parameter P(SWT), which is given by Equation 4.1 (Smith *et al.* 1970), where σ_a , σ_m, ε_a and E are rispectively the stress amplitude, mean stress, strain amplitude and Young's modulus of the material.

$$P(SWT) = \sqrt{(\sigma_a + \sigma_m)\varepsilon_a E} \tag{4.1}$$

Assuming for the FEM model that the process has linear elastic behaviour, as in section 2.6, then the stress becomes proportional to the strain. Under this hypothesis, the P(SWT) parameter can be calculated in terms of strain (converting stress to strain and ignoring E), as shown in Equation 4.2.

$$P(SWT) = \sqrt{(\varepsilon_a + \varepsilon_m)\varepsilon_a} \tag{4.2}$$

This parameter was used to compare results on strain obtained from the present analysis with results obtained from data collected by Dooley in her thesis: present results appeared to have higher maximum strains and lower strain amplitudes than Dooley's results, and the use of the P(SWT) parameter allowed for a reasonable comparison.

The Smith Watson Topper parameter was therefore calculated for each process and plotted against the number of cycles experienced before its rupture (Figure 4.1). As compressive cycles were not constant (both the strain amplitude and the mean strain varied from one cycle to the next) average values were used to calulate the P(SWT) parameter.

From this analysis resulted that the P(SWT) parameter decreases in its value as the number of cycles to failure for an osteocyte process increases, in completely similarity with the strain range experienced by the process and the crack displacement range in its vicinity.

The P(SWT) parameter is an empirical law by Smith *et al.* which is generally used in industry for metallic materials: we did not know if it was appropriate for

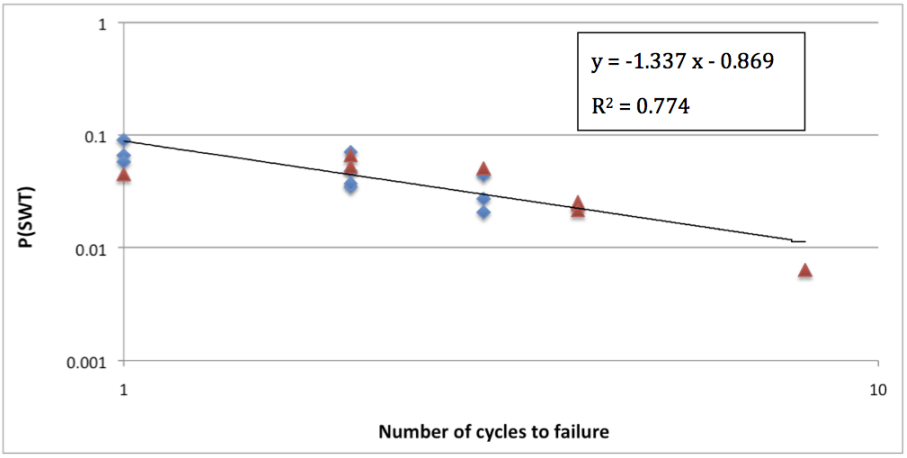

Figure 4.1. This graph shows the P(SWT) parameter plotted against the number of cycles to failure. Results obtained from Dooley's thesis are included in this graph (red triangles in the graph).

cells, too. Comparing Figure 4.1 and Figure 3.9 it can be noticed that plotting the P(SWT) parameter allows for less scatter than plotting the strain range over the number of cycles to failure.

The R^2 value computed in Excel determines how closely data conform to a linear relationship. R^2 values range from 0 to 1, with 1 representing a perfect fit between the data and the line drawn through them, and 0 representing no statistical correlation between the data and a line. The R^2 value (often referred to as the goodness of fit) is computed as shown in Equation 4.3, where Y_i represents an individual data point value, Y_i' represents the value obtained by when the independent coordinate of this data point is input into the best-fit function (a line in the present case).

$$R^2 = 1 - \frac{\sum(Y_i - Y_i')^2}{\sum(Y_i - \bar{Y})^2} \tag{4.3}$$

As the R^2 values for strain range linear fit, i.e. 0.562, is lower than the R^2 value for the P(SWT) parameter, i.e. 0.774, the Smith Watson Topper parameter can be a successful instrument to allow for the different mean stresses in the osteocyte processes analysis.

There are important differences between Dooley's tests and the present study: in the present tests we were focusing on cracks already formed *in vivo*, applying a stress of 36 MPa parallel to the longitudinal axis of bone. Dooley focused on artefacts cracks, with no *in vivo* previous loading, applying a stress of 18 MPa perpendicularly to the longitudinal axis of bone.

Because of its anisotropic behaviour, bone shows higher resistance to loading along its longitudinal axis, being the longitudinal Young's modulus 22 GPa, while the transverse Young's modulus is 15 GPa (Reilly and Burstein 1975). At the same time, considering microcrack orientation in bone, being the average inclination of a microcrack 70° to the longitudinal axis of the bone (Taylor *et al.* 2003), it must be taken into account that applying stress parallel to the longitudinal axis will cause crack to displace mainly because of shear stress. Loading samples perpendicularly to the longitudinal axis will cause crack opening mainly due to normal stress, instead.

These differences can justify the variation in process strain amplitudes noticed between the two sets of data: bone reasonably shows to be more resistant (i.e. lower processes strain amplitude) if load is applied on a direction parallel to its longitudinal axis.

The higher maximum level of strain measured in the present study considering processes that failed is due to the fact that to obtain process failure for processes that did not rupture after *in vivo* loading it was necessary to apply reasonably high level of strain. In addition, drying can be responsible of increasing the opening of cracks to displacement values higher than actual *in vivo* values, as discussed in section 4.3. This does not mean that the lower level of strain measured in Dooley's thesis could not have caused process rupture in the present samples, but simply that this could not be revealed through *in situ* testing, because processes that failed at that level of strain probably broke during the *in vivo* straining.

The use of the Smith Watson Topper parameter P(SWT) to combine the strain range and the mean strain allowed not only to state that both analysis show the decreasing of the number of cycles to failure with the increasing of cyclic strain range experienced by osteocyte process, but revealed present results to be coherent with Dooley's data.

This is an important achievement, as present results refer to microcracks in bone loaded in a way comparable to *in vivo* conditions: this allows to extend Dooley's achievements on artefacts cracks to generic microcracks in bone.

It is conventional in fatigue studies to plot these data logarithmically, as shown in the following equation, and to apply a linear trendline, implying the following relationship between cyclic strain ($\Delta\varepsilon$) and the number of cycles to failure (N_f).

$$N_f = \frac{C}{\Delta\varepsilon^n} \tag{4.4}$$

Here C and n are constants. The line shown in Figure 4.1 has a good fit to the data ($R^2 = 0.774$) with the exponent n = 0.82. Compared to data on other materials this is a relatively low value of n, but not unprecedented. Figure 4.2 shows similar data for two metallic materials (Boller and Seeger 1987).

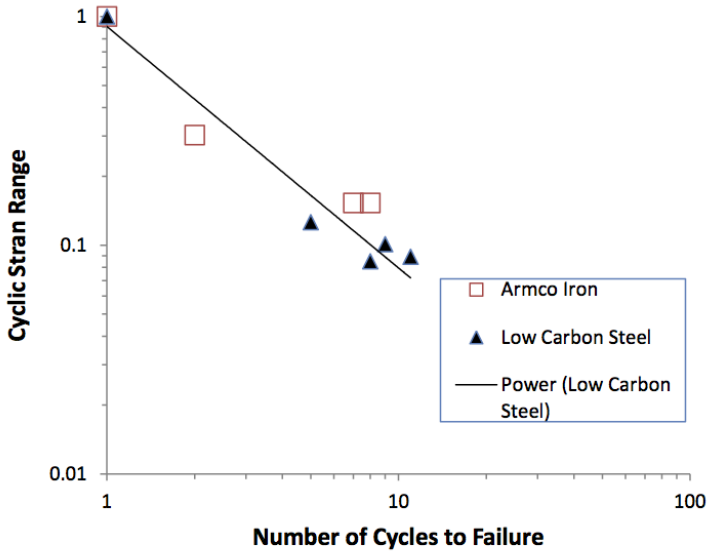

Figure 4.2. This graph shows the number of cycles to failure for two types of metal.

These results provide further support for the "scissors model" of damage detection, albeit in a modified form in which the primary cause of process rupture is cyclic fatigue failure rather than instantaneous cutting. The low value of n in equation 1, and the consequent steep slope of the line on Figure 3.9, has an interesting effect.

Testing bone samples at 80 MPa, which is approximately half the stress needed for instantaneous failure, it was found that most of the cellular processes fails after 100 cycles, whilst the bone matrix itself has an average life of 100,000 cycles (Dooley 2013). This again promotes osteocyte cell process failure as an early warning system for detecting fatigue damage long before the bone itself begins to fail. Previous work by the Trinity College Dublin bone research group has shown that as osteocyte cell networks are ruptured, cell signalling pathways known to stimulate targeted repair in bone are initiated (Mulcahy *et al.* 2011).

Thanks to the use of the FEM model, strain evaluation was introduced in Dooley's work and applied to present results, showing tested processes experienced strains in the range 0.5-25%: strains of this magnitude are known to occur in many type of cells. This is the first study to estimate the cyclic strain range and relate it to the number of cycles to failure, for any type of cell.

Previous studies on the failure strain of cell membrane where perfomed by Nichol and Hutter (1996), who tested sarcolemmal vescicles in order to determine mechanical properties of the surface membrane of skeletal muscle. The fractional increase in membrane area vesicles could sustain before bursting (comparable to the strain level

to failure) was 0.026 ± 0.005 (Nichol and Hutter 1996). This value is comparable to the upper limit of the strain range experienced by processes that broke during *in situ* tests in the present analysis, i.e. 0.025.

Strain level was completely in accordance with crack opening displacement, as believed.

The FEM simulation allowed collecting data on the level of stress experienced by the osteocyte process, considering adhesion to the bone matrix. The theory that the local adhesion between the process and the bone in its vicinity can fail in a determined section of its length after applying load, depending on the stress intensity, was investigated in its consequences.

Stress resulted to be higher in the area of the process in the vicinity of the microcrack, with its intensity reducing while moving further from the crack along the process length. In the present research, we admitted a limit stress value for local adhesion of 7.96 Pa, in accordance with studies from Sheldon *et al.* (Sheldon et al. 2011).

The analysis showed that the section of the process in the proximity of the crack experiences a failure of its adhesion to the bone, while the two extremities of the process remain connected to the bone matrix. The length of the free length resulted proportional to the intensity of stress applied, i.e. to the crack displacement opening.

The increase of the length of the free section with the increase of the stress intensity showed to be a way for osteocyte process to reduce the level of strain it would otherwise experience if completely bounded to the bone, as referred to equation 2.4, which shows the strain to be inversely proportional to the free length of the process.

Finally, the presence of creep behaviour in bone tissue under cyclic applied load was revealed by FEM analysis, in accordance with experimental data and theory from Rimnac *et al.* (Rimnac et al. 1993). In particular, a reasonable explanation to the behaviour of microcrack considering its opening variation during cyclic loading was finally given: the fact that over time the average crack opening in the vicinity of a process tended to decrease but the cyclic displacement range remained approximately constant is due to the effect of creep, not simply to plasticity.

FEM model proved to be a useful and reliable instrument to study crack displacement under loading and consequently the stress and strain levels in the osteocyte process spanning the crack.

4.2 Limitations

The size of osteocyte processes meant a scanning electron microscope was necessary in order to view the dendritic cellular material in a resolution high enough to allow separation of intact and broken osteocyte processes. This meant the sample had to be prepared for the high vacuum environment of an SEM chamber. The samples were dried using alcohol dehydration and a critical point dryer, the most delicate way to dry biological material for an SEM without damaging the structure (Dooley 2013).

Drying could cause the shrinking and cracking of bone. There was a worry that this drying could result in the opening of cracks and the rupture of cell processes due to tensile strain. Drying could be responsible of increasing opening of cracks to displacement values higher than actual *in vivo* values. This may be an explanation to the high opening displacement measured in cracks.

Drying a material affects its properties and there was a fear that drying of the cellular material would have resulted in changes that would make the material more fragile and easier to break. This was addressed by comparing the samples strained in their normal, non fixed, hydrated condition to those strained *in situ* in the SEM.

Dooley showed the processes in both sets of samples had comparable failure rates of 62% (wet, non fixed sample) to 77% (dry, *in situ* strained sample), suggesting that fixation and drying has relatively little effect on the results. Heavy metal staining of the samples was necessary so *in vivo* formed cracks could be distinguished from artefact cracks. The above comparisons also allowed to dismiss this as a limitation to the investigation, as results from stained and non stained sample testing were comparable.

A limitation of this study was the small number of cycles to failure obtained from measurement: up to 3. The possibility of integrating the present results with data from Dooley's thesis by using Smith Watson Topper parameter P(SWT) allowed to obtain more reliable quantification of the strain range necessary for fatigue failure of osteocytes, obtaining experimental values to up to 8 cycles to failure.

The measurement of crack opening was taken from a single area along the microcrack in the vicinity of an intact cell process and so perhaps did not reflect what was happening in the rest of the crack face. The fact that choosing randomly chosen area within different cracks from different samples showed comparable effects considering crack opening displacement allowed to dismiss this as a limitation to the investigation.

Considering the FEM analysis, osteocyte process was modelled as completely elastic, because of lack of experimental data from available literature. This could be a limitation in the evaluation of stress and strain after cyclic applied load as plasticity

and consequently permanent deformation effects may be involved, considering the high strain level processes showed to be exposed to (up to 25%).

The lack of experimental data on the strength of the local adhesion connection between osteocyte process and bone might be a limitation to the present study in determining with precision the free length of a process and consequently strain in process. Considering different values of the limit shear stress for process adhesion may affect the level of strain experienced by process but cannot modify the trend highlighted in the present work: the greater the strain experienced by a process the less cycles to rupture.

4.3 Conclusions

- It is possible for crack opening to change and process rupture to take place in cyclic compressive loading.
- In the majority of cases the mode of osteocyte process rupture is fatigue rather than monotonic rupture due to a single load application.
- The displacement range necessary for fatigue failure of osteocytes has been quantified. The greater the displacement of the microcrack faces the less cycles to process rupture.
- The strain range necessary for fatigue failure of osteocytes has been quantified. In accordance with displacement range, the greater the strain experienced by a process the less cycles to rupture.
- These observations support the "scissors model" as a viable mechanism of microcrack detection by the osteocyte network. Albeit in a slightly modified form where the method of rupture is fatigue resulting from simple cyclic tensile motion and complete microcrack closing does not appear to take place.
- The failure of the focal adhesion between process and bone after applying load shows to be proportional to the intensity of stress experienced by the process: the free length of a process increases as the crack displacement increases.
- Bone shows creep effects under cyclic applied load: it is not possible to limit material properties to plasticity to completely describe the displacement of microcracks subjected to mechanical fatigue.

4.4 Future work

The work included in this thesis tells us about the effect microdamage and compressive cyclic strain has on osteocyte cell's processes. Answering a question usually leads to the formulation of another and this work is no exception.

The continuation of the FEM study is important as it should be improved considering the natural orientation of microcracks in bone, i.e. 70° to the longitudinal axis of the bone. This would lead to a more in depth analysis of the stress and strain experienced by osteocyte processes while bone is loaded in vivo: not only compressive forces act on microcracks in bone but shear forces as well play an important role in determining crack edges displacement.

Further work might include a FEM analysis of the strain level in processes considering different values of the shear stress necessary for process adhesion rupture, as there is very lack of experimental data on the strength of this local adhesion. This may affect the level of strain experienced by process as a consequence of a variation of the dimension of the free length in a process at a certain level of stress.

The present work describes conditions involved in fatigue and rupture, but does not directly address the repair process, which may likely be triggered by the osteocyte injury. Further work may address the biological mechanism involved in the microcracks resolution in order to completely validate the "scissors model" presented by Taylor et al. as a viable mechanism of microcrack detection by the osteocyte network.

Appendix A

References

Anderson, C. T., Castillo, A. B., Brugmann, S. A., Helms, J. A., Jacobs, C. R. and Stearns, T. (2008) 'Primary Cilia: Cellular Sensors for the Skeleton', The Anatomical Record: Advances in Integrative Anatomy and Evolutionary Biology, 291(9), 1074-1078.

Andreson, T. L. (1994) 'Fracture Mechanics: Fundamentals and Applications, Secon Edition', Taylor and Fransis Pub, 104-105, 107-108

Boller, C. and Seeger, T. (1987) 'Materials Data for Cyclic Loading', Publ. Elsevier, Amsterdam, The Netherlands.

Bonewald, L.F. (2007) 'Osteocytes as dynamic multifunctional cells', Ann N Y Acad Sci, 1116, 281–290.

Boyle, W. J., Simonet, W. S. and Lacey, D. L. (2003) 'Osteoclast differentiantion and activation', Nature, 423, 337 - 342.

Boyle, W. J., Simonet, W. S. and Lacey, D. L. (2003) 'Osteoclast differentiantion and activation', Nature, 423, 337 - 342.

Bronner, F. (1992) 'Bone and calcium homeostasis', Neurotoxicology, 13, 775–782

Burr, D. B. and Hooser, M. (1995) 'Alterations to the en bloc basic fuchsin staining protocol for the demonstration of microdamage produced in vivo', Bone, 17(4), 431-433.

Burr, D. B. and Martin, R. B. (1993) 'Calculating the probability that microcracks initiate resorption spaces', Journal of Biomechanics, 26(4–5), 613-616.

Burr, D. B. and Stafford, T. (1990) 'Validity of the bulk-staining technique to separate artifactual from in vivo bone microdamage', Clinical orthopaedics and related research, (260), 305-8.

Burr, D. B. and Stafford, T. (1990) 'Validity of the bulk-staining technique to separate artifactual from in vivo bone microdamage', Clinical orthopaedics and related research, (260), 305-8.

Burr, D. B., Martin, R. B., Schaffler, M. B. and Radin, E. L. (1985) 'Bone remodeling in response to in vivo fatigue microdamage', Journal of Biomechanics, 18(3), 189-200.

Burr, D. B., Turner, C. H., Naick, P., Forwood, M. R. and Pidaparti, R. (1997) 'En bloc staining of bone under load does not improve dye diffusion into microcracks', Journal of Biomechanics, 31(3), 285-288.

Caille N, Thoumine O, Tardy Y, Meister JJ (2002) Contribution of the nucleus to the mechanical properties of endothelial cells. J Bio- mech 35(2):177–187.

Carter, D. R. and Hayes, W. C. (1977) 'Compact bone fatigue damage: a microscopic examination', Clinical orthopaedics and related research, (127), 265-74.

Colopy, S. A., Benz-Dean, J., Barrett, J. G., Sample, S. J., Lu, Y., Danova, N. A., Kalscheur, V. L., Vanderby Jr, R., Markel, M. D. and Muir, P. (2004) 'Response of the osteocyte syncytium adjacent to and distant from linear microcracks during adaptation to cyclic fatigue loading', Bone, 35(4), 881-891.

Costa KD, Sim AJ, Yin FC (2006) Non-Hertzian approach to analyzing mechanical properties of endothelial cells probed by atomic force microscopy. J Biomech Eng 128(2):176–184.

Cowin, S. C., Moss-Salentijn, L. and Moss, M. L. (1991) 'Candidates for the Mechanosensory System in Bone', Journal of Biomechanical Engineering, 113(2), 191-197.

Currey, J.D. (2003) 'The many adaptations of bone', J Biomech, 36, 1487–1495

Currey, J. D. (2002) 'Bones: Structure and Mechanics', Princeton University Press, Ch. 1, 4.

Deguchi S, Maeda K, Ohashi T, Sato M (2005) Flow-induced hardening of endothelial nucleus as an intracellular stress-bearing organelle. J Biomech 38(9):1751–1759.

Dooley, C. M. (2013), 'Targeted Bone Remodelling: Investigating the Scissors Model', A thesis submitted to the University of Dublin in partial fulfilment of the requirements for the degree of Doctor of Philosophy, Department of Mechanical and Manufacturing Engineering - Trinity College Dublin

Ducy, P., Schinke, T. and Karsenty, G. (2000) 'The Osteoblast: A Sophisticated Fibroblast under Central Surveillance', Science, 289(5484), 1501.

Dunstan, C. R., Somers, N. M. and Evans, R. A. (1993) 'Osteocyte death and hip fracture', Calcified Tissue International, 53(0), S113-S117.

Ewald, H. L. and Wanhill, R. J. H. (1989) 'Fracture mechanics', Edward Arnold Publishers, Delft.

Feneberg W, Aepfelbacher M, Sackmann E (2004) Microviscoelasticity of the apical cell surface of human umbilical vein endothelial cells (HUVEC) within confluent monolayers. Biophys J 87(2): 1338–1350.

Forwood, M. and Parker, A. (1989) 'Microdamage in response to repetitive torsional loading in the rat tibia', Calcified Tissue International, 45(1), 47-53.

Franz-Odendaal, T.A., Hall, B.K. and Witten, P.E. (2006) 'Buried alive: how osteoblasts become osteocytes', Dev Dyn, 235, 176–190

Frost, H. M. (1960) 'Presence of microscopic cracks invivo in bone', Bulletin of Henry Ford Hospital, 8, 25 - 35.

Frost, H. M. (1987) 'Bone "mass" and the "mechanostat": A proposal', The Anatomical Record, 219(1), 1-9.

Frost, H.M. (1966) 'Bone dynamics in metabolic bone disease', J Bone Jt Surg, 48, 1192–1203

Hazenberg, J. G., Freeley, M., Foran, E., Lee, T. C. and Taylor, D. (2006) 'Microdamage: A cell transducing mechanism based on ruptured osteocyte processes',

Journal of Biomechanics, 39(11), 2096-2103.

Hazenberg, J. G., Freeley, M., Foran, E., Lee, T. C. and Taylor, D. (2006) 'Microdamage: A cell transducing mechanism based on ruptured osteocyte processes', Journal of Biomechanics, 39(11), 2096-2103.

Hazenberg, J. G., Freeley, M., Foran, E., Lee, T. C. and Taylor, D. (2006a) 'Microdamage: A cell transducing mechanism based on ruptured osteocyte processes', Journal of Biomechanics, 39(11), 2096-2103.

Henon S, Lenormand G, Richert A, Gallet F (1999) A new determi- nation of the shear modulus of the human erythrocyte membrane using optical tweezers. Biophys J 76(2):1145–1151.

Janssen, M., Zuidema, J. and Vanhill, R. (2004) 'Fracture Mechanics, Second edition: Fundamentals and Applications', CRC Press, 61-65

Karcher H, Lammerding J, Huang H, Lee RT, Kamm RD, Kaazempur- Mofrad MR (2003) A three-dimensional viscoelastic model for cell deformation with experimental verification. Biophys J 85(5):3336–3349.

Kelly, G. M., Kilpatrick, J., van Es, M. H., Weafer, P. P., Prendergast, P. J. and Jarvis, S. P. (2011) 'Bone cell elasticity and morphology changes during the cell cycle', Journal of Biomechanics, 44, 1484-1490.

Kenzora, J. E., Steele, R. E., Yospovitch, Z. H. and Glimcher, M. J. (1978) 'Experimental Osteonecrosis of the Femoral Head in Adult Rabbits', Clinical orthopaedics and related research, 130, 8-46.

Ker, R.F., Wang, X.T. and Pike, A.V.L. (2000) 'Fatigue quality of mammalian tendons', J. Exp. Biol., 203, 1317–1327.

Kim, D.-H., Wong, P. K., Park, J., Levchenko, A. and Sun, Y. (2009) 'Microengineered Platforms for Cell Mechanobiology', Annual Review of Biomedical Engineering, 11(1), 203-233.

Kurata, K., Fukunaga, T., Matsuda, J. and Higaki, H. (2007) 'Role of mechanically damaged osteocytes in the initial phase of bone remodeling', International Journal of Fatigue, 29(6), 1010-1018.

Lanyon, L. E. (1993) 'Osteocytes, strain detection, bone modeling and remodeling', Calcified Tissue International, 53(0), S102-S107.

Laurent VM, Henon S, Planus E, Fodil R, Balland M, Isabey D, Gallet F (2002) Assessment of mechanical properties of adherent liv- ing cells by bead micromanipulation: comparison of magnetic twisting cytometry vs optical tweezers. J Biomech Eng 124(4):

Lee, T. C., O'Brien, F. J. and Taylor, D. (2000) 'The nature of fatigue damage in bone', International Journal of Fatigue, 22(10), 847-853.

Lynch, M. P., Capparelli, C., Stein, J. L., Stein, G. S. and Lian, J. B. (1998) 'Apoptosis during bone- like tissue development in vitro', Journal of Cellular Biochemistry, 68(1), 31-49.

Malone, A. M. D., Anderson, C. T., Tummala, P., Kwon, R. Y., Johnston, T. R., Stearns, T. and Jacobs, C. R. (2007) 'Primary cilia mediate mechanosensing in bone cells by a calcium-independent mechanism', Proceedings of the National Academy of Sciences, 104(33), 13325-13330.

Manolagas, S.C. (2006) 'Choreography from the tomb: an emerging role of dying osteocytes in the purposeful, and perhaps not so purposeful, targeting of bone remodeling', BoneKEy-Osteovision, 3, 5–14

Marotti, G. (1996) 'The structure of bone tissues and the cellular control of their deposition', Ital J Anat Embryol=Arch Ital Anat Embryol, 101, 25–79

Marotti, G., Muglia, M.A. and Palumbo, C. (1994) 'Structure and function of lamellar bone', Clin Rheumatol, 13(Suppl 1), 63–68

Matthews BD, Overby DR, Alenghat FJ, Karavitis J, Numaguchi Y, Allen PG, Ingber DE (2004) Mechanical properties of individual focal adhesions probed with a magnetic microneedle. Biochem Biophys Res Commun 313(3):758–764.

McNamara, L. M., Majeska, R. J., Weinbaum, S., Friedrich, V. and Schaffler, M. B. (2009) 'Attachment of Osteocyte Cell Processes to the Bone Matrix', The Anatomical Record, 292, 355–363.

Melanotte, P. L. and Follis, R. H. (1961) 'Early Effects of X-Irradiation on Cartilage and Bone', Americal journal of pathology, 39(1), 1 - 15.

Miller, S. and Jee, W. (1987) 'The bone lining cell: A distinct phenotype?', Calcified Tissue International, 41(1), 1-5.

Mori, S. and Burr, D. B. (1993) 'Increased intracortical remodeling following fatigue damage', Bone, 14(2), 103-109.

Mori, S., Harruff, R., Ambrosius, W. and Burr, D. B. (1997) 'Trabecular bone volume and microdamage accumulation in the femoral heads of women with and without femoral neck fractures', Bone, 21(6), 521-526.

Mullender, M.G., van der Meer, D.D., Huiskes, R. and Lips, P. (1996) 'Osteocyte density changes in aging and osteoporosis', Bone, 18, 109–113

Neve, A., Corrado, A. and Cantatore, F. P. (2011) 'Osteoblast physiology in normal and pathological conditions', Cell Tissue Research, 343(2), 289 - 302.

Nichol, J.A. and Hutter, O.F. (1996) 'Tensile strength and dilatational elasticity of giant sarcolemmal vesicles shed from rabbit muscle', Journal of Physiology, 493, 187-198.

Nicolella, D. P., Moravits, D. E., Gale, A. M., Bonewald, L. F. and Lankford, J. (2006) 'Osteocyte lacunae tissue strain in cortical bone', Journal of Biomechanics, 39(9), 1735-1743.

Noble, B. S. and Reeve, J. (2000) 'Osteocyte function, osteocyte death and bone fracture resistance', Molecular and Cellular Endocrinology, 159(1–2), 7-13.

Noble, B. S., Stevens, H., Loveridge, N. and Reeve, J. (1997) 'Identification of apoptotic changes in osteocytes in normal and pathological human bone', Bone, 20(3), 273-282.

Noble, B.S. (2008) 'The osteocyte lineage', Arch Biochem Biophys, 473, 106–111

Overby DR, Matthews BD, Alsberg E, Ingber DE (2005) Novel dynamic rheological behavior of individual focal adhesions measured within single cells using electromagnetic pulling cytometry. Acta Biomater 1(3):295–303.

Palumbo, C., Palazzini, S., Zaffe, D. and Marotti, G. (1990) 'Osteocyte differentiation in the tibia of newborn rabbit: an ultrastructural study of the formation of cytoplasmic processes', Acta Anat, 137, 350–358

Qiu, S. J., Boyce, T. M. and Schaffler, M. B. (1997) 'Osteocyte loss and microdamage in aging human compact bone', Trans Orthop Res Soc, 22, 88.

Radmacher, M. (1997) 'Measuring the elastic properties of biological samples with the AFM.' IEEE Eng. Med. Biol. Mag., 16, 47-57.

Rand, R. P. and Burton, A. C. (1964) 'Mechanical Properties of the Red Cell Membrane: I. Membrane Stiffness and Intracellular Pressure', Biophysical Journal, 4(2), 115-135.

Reilly, D.T. and Burstein, A. H. (1975) 'The elastic and ultimate properties of compact bone tissue', J. Biomechanics , 8, 393-405, 1975

Reilly, G. C. (2000) 'Observations of microdamage around osteocyte lacunae in bone', Journal of Biomechanics, 33(9), 1131-1134.

Reilly, G. C. and Currey, J. D. (1999) 'The development of microcracking and failure in bone depends on the loading mode to which it is adapted', Journal of Experimental Biology, 202(5), 543-552.

Rubin, C. (1984) 'Skeletal strain and the functional significance of bone architecture'

Sato H, Kataoka N, Kajiya F, Katano M, Takigawa T, Masuda T (2004) Kinetic study on the elastic change of vascular endothelial cells on collagen matrices by atomic force microscopy. Colloids Surf B Biointerfaces 34(2):141–146

Schaffler, M. (2003) 'Role of bone turnover in microdamage', Osteoporosis International, 14(0), 73-80.

Schaffler, M. B., Burr, D. B. and Radin, E. L. (1989) 'Mechanical and morphological effects of strian rate on fatigue in compact bone', Bone, 10, 207 - 214.

Schaffler, M. B., Pitchford, W. C., Choi, K. and Riddle, J. M. (1994) 'Examination of compact bone microdamage using back-scattered electron microscopy', Bone, 15(5), 483-488.

Schrot S, Weidenfeller C, Schaffer TE, Robenek H, Galla HJ (2005) Influence of hydrocortisone on the mechanical properties of the cerebral endothelium in vitro. Biophys J 89(6):3904–3910.

Seeman, E. (2006) 'Osteocytes—martyrs for integrity of bone strength', Osteoporosis International, 17(10), 1443-1448.

Sheldon, M. W., Young-Hun, C., Carl, G. S., Jackson, C., Yan, D. and Delbert, D. (2011) 'Cell adhesion to borate glasses by coloidal probe microscopy', Acta Biomaterialia, 7, 2256-2263.

Smith, K. N., Watson, P. and Topper, T. H. (1970) 'A stress-strain function for the fatigue of metals' , J. Mater. ASTM, 5(4). 767-768

Suda, T., Takahashi, N., Udagawa, N., Jimi, E., Gillespie, M. T. and Martin, T. J. (1999) 'Modulation of osteoclast differentiation and function by the new members of the tumor necrosis factor receptor and ligand families', Endocrine Reviews, 20(3), 345-57.

Tada, H., Paris, P. C. and Irwin G. (1985) 'The Stress Analysis of Cracks Handbook', Del Research Corporation, 408-421

Taylor, D. (1997) 'Bone maintenance and remodeling: A control system based on fatigue damage', Journal of Orthopaedic Research, 15(4), 601-606.

Taylor, D., Casolari, E. and Bignardi, C. (2004) 'Predicting stress fractures using a probabilistic model of damage, repair and adaptation', Journal of Orthopaedic Research, 22(3), 487-494.

Taylor, D., Hazenberg, J. G. and Lee, T. C. (2003) 'The cellular transducer in damage- stimulated bone remodelling: a theoretical investigation using fracture mechanics', Journal of Theoretical Biology, 225(1), 65-75.

Taylor, D., Hazenberg, J. G. and Lee, T. C. (2003) 'The cellular transducer in damage-stimulated bone remodelling: a theoretical investigation using fracture mechanics', Journal of Theoretical Biology, 225(1), 65-75.

Taylor, D., Hazenberg, J. G. and Lee, T. C. (2003) 'The cellular transducer in

damage-stimulated bone remodelling: a theoretical investigation using fracture mechanics', Journal of Theoretical Biology, 225, 65-75

Temiyasathit, S. and Jacobs, C. R. (2010) 'Osteocyte primary cilium and its role in bone mechanotransduction', Annals of the New York Academy of Sciences, 1192(1), 422-428.

Vashishth, D., Behiri, J. C. and Bonfield, W. (1997) 'Crack growth resistance in cortical bone: Concept of microcrack toughening', Journal of Biomechanics, 30(8), 763- 769.

Vatsa, A., Breuls, R.G., Semeins, C.M., Salmon, P.L., Smit, T.H. and Klein-Nulend, J. (2008) 'Osteocyte morphology in fibula and calvaria— is there a role for mechanosensing?', Bone, 43, 452–458

Verborgt, O., Gibson, G. J. and Schaffler, M. B. (2000) 'Loss of Osteocyte Integrity in Association with Microdamage and Bone Remodeling After Fatigue In Vivo', Journal of Bone and Mineral Research, 15(1), 60-67.

Wang N, Ingber DE (1995) Probing transmembrane mechanical cou- pling and cytomechanics using magnetic twisting cytometry. Biochem Cell Biol 73(7–8):327–335

You, L., Temiyasathit, S., Lee, P., Kim, C. H., Tummala, P., Yao, W., Kingery, W., Malone, A. M., Kwon, R. Y. and Jacobs, C. R. (2008) 'Osteocytes as mechanosensors in the inhibition of bone resorption due to mechanical loading', Bone, 42(1), 172-179.

You, L., Temiyasathit, S., Lee, P., Kim, C. H., Tummala, P., Yao, W., Kingery, W., Malone, A. M., Kwon, R. Y. and Jacobs, C. R. (2008) 'Osteocytes as mechanosensors in the inhibition of bone resorption due to mechanical loading', Bone, 42(1), 172-179.

Zeng, D., Juzkiw, T., Read, A. T., Chan, D. W.-H., Glucksberg, M. R., Ethier, C. R. and Johnson, M. (2010) 'Young's modulus of elasticity of Schlemm's canal endothelial cells', Biomech Model Mechanobiol, 9, 19–33.

Zhang, P., Su, M., Tanaka, S.M. and Yokota, H. (2006) 'Knee loading stimulates cortical bone formation in murine femurs', BMC musculoskeletal disorders, 7, 73